Authors

Aileen Schmidt[1,2], Laurien Czichon[1,2], Leonie Malhofer[1,2], Gioia Bartsch[1,2], Clara Plötner[1,2], Yuepeng Wang[1,2], Carola Voss[1,2], Anna Kuleshova[1,2], Tim Kohrn[1,2], Julia Baldauf[4], Astrid Weiß[4], Ralph Schermuly[4], Arjang Ruhparwar[1,2], Jan C. Kamp[2,3], Marius M. Hoeper[2,3], Ulrich Martin[1,2*,+], Ruth Olmer[1,2*,+]

Affiliations

[1] Leibniz Research Laboratories for Biotechnology and Artificial Organs (LEBAO), Clinic for Cardiothoracic-, Transplantation and Vasuclar Surgery, Hannover Medical School, Hannover, Germany

[2] Biomedical Research in Endstage and Obstructive Lung Disease (BREATH), German Center for Lung Research (DZL), Hannover Medical School, Hannover, Germany

[3] Department of Respiratory Medicine and Infectious Diseases, Hannover Medical School (MHH), Hannover, Germany

[4] Department of Internal Medicine, Justus Liebig University of Giessen, Institute for Lung Health, Giessen, Germany.

* contributed equally, [+]corresponding author

Title

iPSC modeling of pulmonary arterial hypertension to uncover pathomechanisms and unrecognized modes of action of sotatercept

Graphical abstract

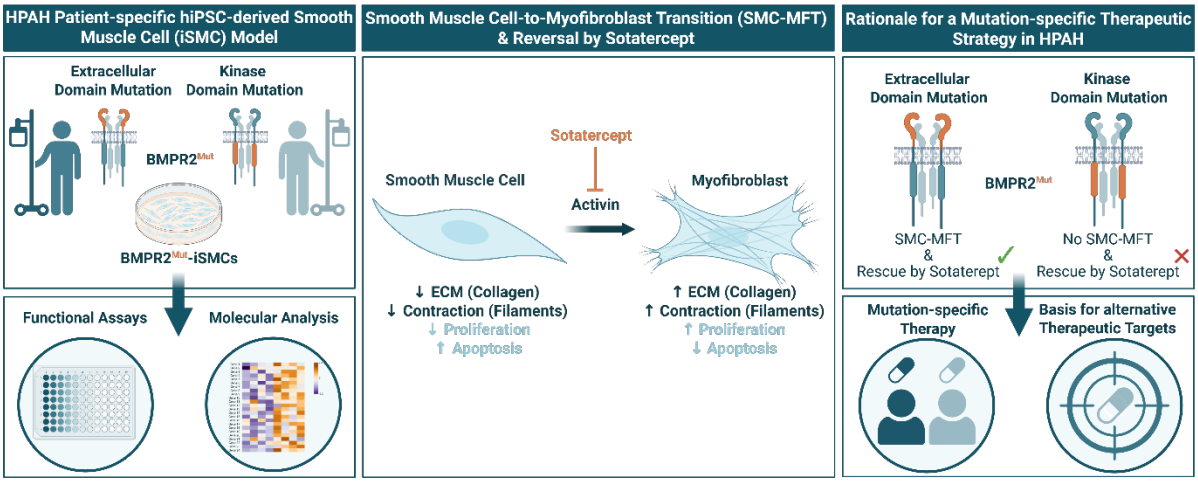

Abstract

Pulmonary arterial hypertension (PAH) is a potentially fatal disease characterized by obliterative remodeling of distal pulmonary arteries, commonly associated with bone morphogenetic receptor type 2 (BMPR2) gene mutations. In patients with PAH, sotatercept, an activin signaling inhibitor, improves hemodynamics and outcomes, but clinical responses vary and sometimes occur within weeks, suggesting additional mechanisms beyond its anti-proliferative, pro-apoptotic and anti-remodeling effects.

Using patient-specific induced pluripotent stem cell-derived smooth muscle cells (iSMCs) with BMPR2 extracellular- or kinase-domain mutations, we were able to reproduce Activin A-driven PAH traits, including hyperproliferation, reduced apoptosis, enhanced contraction and excessive matrix production.

We identified smooth muscle cell-to-myofibroblast transition as a previously unknown contributor to pulmonary vascular remodeling and demonstrate that it is blocked by sotatercept.

Beyond its established effects, sotatercept rapidly reduced contractility, collagen-integrin mechanotransduction and TGFβ receptor expression, disrupting a pathological positive feedback loop, reflected by lower levels of circulating TGFβ1 in patients on sotatercept.

Taken together, our patient-derived iSMC platform links mutation-dependent mechanisms of pulmonary vascular remodeling to variable drug responsiveness and reveals previously unrecognized, potentially rapid-acting modes of sotatercept in PAH.

Introduction

Heritable pulmonary arterial hypertension (HPAH) is a severe lung vasculopathy involving narrowed lumens, increased resistance and blood pressure within the pulmonary vasculature. This leads to elevated right ventricular afterload and, over time, right heart failure [1]. HPAH is driven by pulmonary vascular remodeling, which is associated with hyperproliferation [2], apoptosis resistance [3], hypercontraction [4], and dysregulated extracellular matrix (ECM) deposition [5,6] of vascular cells.

In HPAH, pathogenic variants in the bone morphogenetic protein receptor type 2 (BMPR2) encoding gene are present in 80% of patients [7], leading to more severe symptomatology, increased mortality, and higher need of lung transplantation [8] compared to patients with idiopathic PAH. BMPR2 deficiency results in maladaptation of the Activin / -TGFβ signaling, which subsequently leads to an imbalance between the canonical SMAD and SMAD-independent pathways [9]. However, the penetrance of *BMPR2* mutations is incomplete. Only about 20–30% of carriers manifest the disease, suggesting that a single genetic defect is insufficient for disease development. The observation that only a minority of individuals with predisposing genetic mutations develop PAH has supported the second hit hypothesis in PAH, according to which second hits (e.g., inflammation, hypoxia or drug exposure) a initiate the pathological process via production of Activin A by immune cells and endothelial cells [10], trigger endothelial dysfunction, promote abnormal smooth muscle proliferation, and contribute to vascular remodeling, ultimately resulting in PAH [11]. At the molecular level, Activin A and BMP 9/10, which can activate SMAD2/3 signaling via binding to a heteromer of ACTR2A/B and TGFβ type-I-receptors (Activin receptor like kinases, ALKs), are key triggers during the initiation and maintenance of the pathological processes underlying PAH [12].

Sotatercept, a novel drug recently approved by the FDA for the treatment of PAH, is a recombinant fusion protein functioning as an Activin/ BMP ligand trap which inhibits Activin/ BMP signaling and rebalances canonical SMAD signaling [13]. This mitigates hyperproliferation and apoptosis resistance in vascular cells and may reverse pulmonary vascular remodeling

processes [14,15]. In clinical studies, sotatercept treatment has shown beneficial effects on haemodynamics, right heart function, and clinical outcomes, with improvement in clinical parameters and endpoints as early as week 3, reaching statistical significance by week 24 after therapy initiation [1,16]. Although preclinical studies suggest that sotatercept's efficacy may be driven at least in part by reverse-remodeling effects, sotatercept's mechanism of action (MoA) in human disease is still incompletely understood. In addition, individual treatment response to sotatercept is variable ranging from normalization or near-normalization of pulmonary hemodynamics to no improvement at all. This heterogeneous response may reflect the contribution of varying pathomechanisms that depend on individual pathogenic mutations and may also suggest unrecognised MoAs of sotatercept.

Due to the limited number of patients and their heterogeneity regarding disease status, medication, co-morbidities, age, gender, nutrition, and other factors, clinical data alone will not sufficiently enable a comprehensive understanding of the pathomechanisms of PAH and the observed variations in drug responsiveness. Various *in vitro* and *in vivo* PAH models have been developed over time; however, they all possess significant limitations [17] and suffer from limited translational relevance [18].

To overcome these shortcomings, we have developed a novel *in vitro* model based on patient-derived induced pluripotent stem cells (iPSCs) that harbor mutations in various domains of the *BMPR2* gene. In contrast to recently established iPSC models of PAH that focus on endothelial cells (ECs) [19,20], our model builds on iPSC-derived smooth muscle cells (iSMCs), which we consider the key cell type involved in the arterial remodeling characteristic of PAH [21]. Taking advantage of the defined conditions of this *in vitro* model, we aim to enhance our understanding of the molecular pathophysiology of PAH and to explore potential unrecognized MoAs of sotatercept. This approach intends to rationalize the heterogeneous responses to treatment observed among PAH patients and to pave the way for a more knowledge-based and individualized approach to PAH therapy.

Results

BMPR2^{Mut} iSMCs show PAH hallmarks of increased proliferation and decreased apoptosis, and recapitulate clinical drug responsiveness

By applying a multistep differentiation protocol, iSMCs were generated from healthy iPSCs (wildtype, WT) and from PAH patient-derived iPSCs, which carry heterozygous BMPR2 mutations. This enabled the modelling of HPAH phenotypes *in vitro* (Fig. 1 A). To exclude clonal artefacts and represent biological variability, three independent WT iPSC lines (BMPR2^{WT}) derived from healthy individuals were utilized, alongside three iPSC clones generated from two patients carrying either a mutation in the extracellular domain (BMPR2^{MutExDo}, heterozygous in-frame-deletion c.248-1 – 418+1 of exon 3 in the extracellular domain) or a mutation in the kinase domain (BMPR2^{MutKiDo}, heterozygous missense mutation c.1471C>T in exon 11 in the kinase domain). Generated iSMC from BMPR2^{WT} or BMPR2^{Mut}-iPSCs were highly enriched and expressed high levels of the SMC marker CD140b (Fig. 1 B). Both, BMPR2^{WT} and BMPR2^{Mut}-iSMCs recapitulated typical characteristics of vascular SMCs, shown by the expression of contractile components such as alpha- smooth muscle actin (actin), calponin (CNN1), and myosin heavy chain 11 (MYH11) (Fig. 1C). Global comparison of the generated iSMCs to publicly available expression data sets of primary vascular SMCs demonstrated a high degree of similarity between iSMCs and isolated primary SMCs (pSMCs), as quantified by a SMC score (Fig. 1 D). Principal Component Analysis (PCA) of RNAseq data from BMPR2^{WT} cell lines and BMPR2^{Mut}-iSMCs clones revealed clustering within respective groups (Fig. 1 E). Nonetheless, the BMPR2^{WT} and BMPR2^{Mut} groups clustered separately, indicating possible HPAH-related differences in gene expression patterns.

An increase in proliferation coupled with a decrease in apoptosis are recognized as hallmarks of PAH [22] and have previously been observed across various models [23]. To verify whether our model recapitulates these *in vitro* phenotypes, proliferative activity and apoptosis rates following Activin A stimulation were analyzed in iSMCs derived from WT and BMPR2^{Mut} iPSC lines. Activin A, a ligand in the TGFβ signaling pathway, is elevated in PAH patients and is a

known trigger of PAH disease progression [9]. While BMPR2^{MutKiDo} iSMCs, exhibited only a trend towards increased proliferation compared to WT cells, BMPR2^{MutExDo} iSMCs showed significantly elevated proliferation (Fig. 1 F). Furthermore, both variants of BMPR2^{Mut} iSMCs revealed significantly reduced caspase activity compared to BMPR2^{WT} iSMCs (Fig. 1 G).Based on recently collected clinical data concerning the recombinant Activin receptor 2A fusion protein, sotatercept [16], our objective was to further validate our *in vitro* system, particularly regarding drug responsiveness. A significant reduction in proliferation and an increase in apoptosis after co-treatment of Activin A-stimulated BMPR2^{Mut}iSMCs with sotatercept reaffirmed the established anti-proliferative and pro-apoptotic MoA of this drug, consistent with observations in other models [24] (Fig. 1 F, G).

The forementioned results from functional assays were corroborated by gene set enrichment analyses based on bulk RNAseq data derived from generated iSMCs (Suppl. Fig. 1, 2). An inhibitory effect of sotatercept on PAH associated pro-proliferative genes, such as MYC proto-oncogene (MYC) [25], marker of proliferation (MKI67) [26], and proliferating cell nuclear antigen (PCNA) [27,28], in BMPR2^{Mut}-iSMCs was confirmed, particularly for BMPR2^{MutExDo}iSMCs (Suppl. Fig. 1). Additionally, PAH associated pro-apoptotic genes, including caveolin-1 (CAV-1) [29] and caspase-4/9 (CASP4/9) [30], were upregulated by sotatercept in BMPR2^{Mut} iSMCs (Suppl. Fig. 2). These findings further underline that our PAH iSMC model recapitulates characteristic PAH phenotypes and is appropriate for conducting drug response studies *in vitro*.

Inhibition of Activin A-induced SMC contraction - an unrecognized MoA of Sotatercept

Hypercontractile SMCs are a central contributor to vessel stiffness and disease progression in patients with PAH [4]. By employing a functional contraction assay, the vasoconstrictive phenotype of the iSMCs was examined (Fig. 2 A, B). While no contraction was observed in any of the vehicle-treated samples, Activin A-stimulated BMPR2^{Mut} iSMCs showed increased responsiveness and contractility when compared to Activin A-stimulated BMPR2^{WT}iSMCs,

thereby recapitulating the proposed *in vivo* phenotype of increased vasoconstriction associated with PAH[31].

The contractile activity of SMCs is directly influenced by the level of phosphorylated myosin light chain (pMLC), which activates the actin-myosin cross-bridge cycle, and is supposed to be alleviated in PAH patients [32,33]. Quantification of the ratio of phosphorylated to non-phosphorylated MLC indicated a tendency towards an increased proportion of pMLC in Activin A stimulated BMPR2^{MutExDo} iSMCs compared to Activin A-stimulated BMPR2^{WT} iSMCs, although statistical significance was not attained. Interestingly, the Activin ligand trap sotatercept has not been associated with any effects on vasoconstriction *in vitro* studies, animal studies, or clinical trials. Consequently, we investigated such effects within our HPAH iSMC model. Remarkably, co-administration of sotatercept significantly reduced the proportion of pMLC in Activin A stimulated BMPR2^{MutExDo} iSMCs (Fig. 2 C). However, in BMPR2^{MutKiDo} iSMCs, which exhibited a less pronounced increase in contractility relative to WT cells, no increase in the ratio of phosphorylated to non-phosphorylated MLC was observed following Activin A treatment, and sotatercept did not diminish the proportion of pMLC.

To further elucidate the effect of sotatercept on SMC contractility, the composition of the contractile apparatus was analyzed, including actin filaments and actin-bound calponin (CNN1), which are essential for the fine-tuning of actin-myosin cross-bridging [34]. Immunofluorescence (IF) staining and protein quantifications demonstrated elevated levels of actin in BMPR2^{Mut} iSMCs following Activin A treatment, with a particularly pronounced increase in BMPR2^{MutExDo} iSMCs (Fig. 2 D, E). Consistent with the contraction assay results, CNN1 was upregulated in BMPR2^{MutExDo}iSMCs after Activin A treatment compared to WT cells, although this was not observed in BMPR2^{MutKiDo} iSMCs (Fig. 2 F, G). Furthermore, in line with the contraction assay findings, sotatercept significantly reduced levels of actin and CNN1 in Activin A-stimulated BMPR2^{MutExDo} iSMCs.

A gene set enrichment analysis was performed to further explore the molecular mechanisms underlying the effect of sotatercept on SMC contraction (Fig. 2 H, I). Although the effect was

more prominent in Activin A-treated BMPR2^{MutExDo} iSMCs, sotatercept appears to exert its anti-contractile effect by downregulating the expression of positive regulators of SMC contraction. For instance, sotatercept reduced the expression of genes associated with PAH, such as myosin heavy chain 11 (MYH11) [35], actin (ACTA2) [9], calponin (CNN1) [27], transgelin (TAGLN) [36], as well as other critical genes involved in SMC contraction, including myosin light chain 9 (MYL9) [37] and smoothelin (SMTN) [38], in both BMPR2^{Mut} iSMCs.

SMC-to-Myofibroblast transition (SMC-MFT) contributes to arterial tissue remodeling in PAH

Increased hydrodynamic parameters and vessel stiffness attributed to heightened ECM content have been documented in patients with PAH [5]. Myofibroblasts are regarded as the main producers of ECM during the pathological tissue remodeling in PAH [39,40]. While it has been proposed that, in the case of PAH, such cells originate from local endothelial cells via endothelial-to-mesenchymal transition (EndoMT) [41], or are derived from quiescent resident fibroblasts or bone marrow-derived circulating cells [39,40], we questioned whether myofibroblasts could also arise from our highly enriched BMPR2^{Mut} iSMCs cultures, serving as an *in vitro* counterpart of BMPR2^{Mut} local arterial SMCs. Given the significant involvement of collagen I in pathological tissue remodeling in PAH and considering that it is typically produced at elevated levels by myofibroblasts, we examined collagen I production following Activin A stimulation of BMPR2^{Mut} iSMCs. In comparison to Activin A-stimulated BMPR2^{WT}iSMCs, an increased expression of collagen I was observable in Activin A stimulated BMPR2^{Mut} iSMCs, which likewise exhibited co-expression of actin, a marker known to be expressed in SMCs and myofibroblasts [42]. In particular, in Activin A-treated BMPR2^{MutExDo}iSMCs, a dense network of collagen I fibers was evident (Fig. 3 A). Quantitative analysis of collagen content per cell revealed a significantly elevated amount of collagen in Activin A stimulated BMPR2^{Mut}-iSMCs relative to the Activin A-stimulated BMPR2^{WT}iSMCs (Fig. 3 B). RNASeq analyses further confirmed a substantial upregulation of various additional genes involved in ECM production,

particularly in Activin A-treated BMPR2^{MutExDo} iSMCs (Fig. 3C). These included collagen I [43], ITGA2 (42), TGFβ1 (43), TGFβR1 (44), as well as ECM-associated genes such as fibronectin (FN1) [44] and tenascin (TNC) [45], all of which are linked to PAH.

The concurrent presence of contractile and ECM features in Activin A treated BMPR2^{Mut} iSMCs prompted us to further explore the molecular signature of Activin A treated BMPR2^{Mut} iSMCs. We observed global similarities to myofibroblasts and fibroblasts in Activin A-treated BMPR2^{Mut} iSMCs from a functional enrichment analysis of bulk RNAseq data (Fig. 3 D). Additionally, an integration of three independent databases, comprising a shared set of approximately 100 genes, identified a robust enrichment of a myofibroblast signature in Activin A-treated BMPR2^{MutExDo} iSMCs. The enrichment was less pronounced in BMPR2^{MutKiDo} iSMCs when compared to Activin-treated BMPR2^{WT} iSMCs (Fig. 3 E).

Interestingly, sotatercept also rescued the elevated expression of various core myofibroblast markers, including platelet-derived growth factor receptor alpha/beta (PDGFRA/B) [46], actin alpha 2 (ACTA2) [40,46], collagen type I alpha 1 chain (COL1A1) [47], fibronectin 1 (FN1) [47,48], caldesmon 1 (CALD1) [48], cadherin 2 (CDH2) [48], calponin 1 (CNN1) [49,50], microfibril-associated glycoprotein 5 (MFAP5) [51,52], tenascin C (TNC) [50], transgelin (TAGLN) [53], and monooxygenase, DBH-like (MOXD1) [54] in Activin A–treated BMPR2^{Mut} iSMCs (Fig. 3F).

Activin A induces mechano-signaling / TGFβ signaling in BMPR2^{Mut} iSMCs

It is well established that accumulated ECM proteins mechanotransduce signals via integrin complexes (ITGA/B), hereby contributing to a positive feedback loop [55] that promotes vascular remodeling in pulmonary hypertension [56,57]. Given the observed elevated expression of collagen I (Fig. 3 A, B) and TGFβ1 (Fig. 3 C) in myofibroblasts derived from Activin A treated BMPR2^{Mut} iSMCs, we hypothesized that there may also be an enhanced collagen-integrin mechano-signaling leading to continuous release of collagen-bound TGFβ1. This might further

stimulate canonical and non-canonical SMAD pathways in the $BMPR2^{Mut}$ SMC derived myofibroblasts, thereby contributing to vascular remodeling.

To explore whether TGFβ1 contributes to PAH severity and drug responsiveness in patients with *BMPR2* mutations, we analyzed serum TGFβ1 levels in such PAH patients before and on sotatercept therapy. Interestingly, elevated TGFβ1 levels in PAH patients significantly decreased with sotatercept therapy (Figure 4 A). To further support the above hypothesis, we analyzed the expression of the collagen I corresponding integrin receptor subunit 2A (ITGA2) in Activin A treated $BMPR2^{Mut}$ iSMCs. Indeed, ITGA2 expression was significantly increased in Activin A stimulated $BMPR2^{MutExDo}$ iSMCs compared to the Activin A-stimulated $BMPR2^{WT}$ iSMCs, while no upregulation was detectable on $BMPR2^{MuKiDo}$ iSMCs (Fig. 4 B, C). Additionally, TGFβR1, which – following tetramerisation with ACTR2 or TGFβR2 – is responsible for signal transduction via SMAD and non-SMAD signaling [58], was significantly upregulated in Activin A-stimulated $BMPR2^{MutExDo}$ iSMCs compared to the Activin A stimulated $BMPR2^{WT}$ iSMCs. Controversially, no upregulation was detectable in $BMPR2^{MutKiDo}$ iSMCs upon Activin A stimulation (Fig. 4 D, E). Remarkably, sotatercept not only largely rescued the increased collagen I protein expression in $BMPR2^{MutExDo}$ iSMCs but also resulted in a significant downregulation of the integrin receptor subunit 2A and TGFβR1 in $BMPR2^{MuExDo}$ iSMCs compared to cells treated with Activin A. Such effects were not observed in $BMPR2^{MuKiDo}$ iSMCs (Fig. 4 B – E). Consequently, sotatercept may also counteract the Activin A induced mechano-signaling-mediated and TGFβ-driven positive feedback loop involved in PAH pathogenesis (Fig. 5).

Discussion

Despite extensive clinical and experimental research, the molecular pathomechanisms of PAH have largely remained unclear until now. Several factors have prevented a deeper understanding of the disease. It is extremely challenging to draw conclusions from clinical data, even in multicenter clinical trials, due to the relatively small and highly heterogeneous patient population, which carries different mutations and shows diverse phenotypes and drug

responsiveness. PAH research is further complicated by the fact that patient's cells and histological specimens are almost exclusively derived from few autopsies or explants after lung transplantation.

Until very recently [59], traditional animal models in rats, and especially mice did not reflect the severity and the genetic causes of the human disease or sex-related differences in prevalence. Even in the era of targeted genetic engineering via CRISPR-Cas, the generation of genetically engineered rats remains laborious, time-consuming, expensive, and the introduction of a multitude of numerous diverse mutations is impractical. Moreover, it is generally difficult to replicate the slow progression of PAH *in vitro*, as only minor differences between wild-type and mutated cells are to be expected during the typically short cell culture periods.

The elegance of our iPSC-based system lies in its capacity to eliminate the influence of disease stage, comorbidities, medications, environmental exposures, infections, and other confounding factors. These highly individual factors significantly complicate the analysis of clinical data, obscuring the underlying, mutation-dependent differences in dysregulated pathways and disease phenotypes. Despite the reduced complexity, our iPSC model still incorporates patient-specific genetic features, allowing us to directly correlate our experimental results with data from clinical studies. This includes the observed drug responsiveness of patients with specific mutations. The unlimited expansion potential of iPSCs poses another advantage for PAH research: Unlike primary cells, iPSCs enable the conduct of numerous repetitive experiments necessary to attain statistical significance, even when discerning minor phenotypic differences between WT and mutated cells, which are anticipated in a disease that develops gradually over years rather than days.

Based on preliminary data from our recent clinical trials, we established iPSC lines from two patients that are heterozygous carriers of pathogenic mutations either in the extracellular or in the kinase domain of the *BMPR2*, employing the same reprogramming protocol.

Despite the relatively small differences observed in functional measurements and expression levels, our experiments conducted under well-defined conditions demonstrated high

reproducibility among individual cell clones derived from a single PAH patient. We intentionally minimized complexity by incorporating only one cell type – SMCs in our model. While other models have previously employed patient-specific iPSC-derived ECs [19,20], and addressed the role of ECs during disease initiation, we hypothesized that SMCs are central to understanding the pathological pulmonary arterial remodeling in PAH. Remarkably, the SMC score of our iPSC-derived iSMCs was even higher than that of primary SMCs isolated from human pulmonary arteries, which may be attributed to contamination of primary cells with other cell types, particularly ECs or fibroblasts. As expected, iSMCs differentiated from the three clones established from each patient clustered closely together, whereas the three WT lines from different donors clustered less closely.

The first pivotal step was to recapitulate the hallmarks of PAH, i. e., hyperproliferation and increased resistance to apoptosis. We confirmed increased proliferation following Activin A stimulation in iSMCs differentiated from all three $BMPR2^{MutExDo}$ clones, compared to $BMPR2^{WT}$ lines. Apoptosis was significantly reduced in iSMCs carrying both mutations. Interestingly, co-treatment with Activin A and sotatercept rescued both proliferation and apoptosis, approximately to WT levels.

RNAseq analyses corroborated the findings of the functional assays, as evidenced by the significant upregulation of pro-proliferative genes in $BMPR2^{MutExDo}$ iSMCs. In contrast, $BMPR2^{MutKiDo}$ iSMCs exhibited a notable downregulation of anti-proliferative genes. For both mutations, reduced apoptosis appear to correlate more strongly with the downregulation of pro-apoptotic genes than with the upregulation of anti-apoptotic genes. Our transcriptome analyses provide additional support for the findings related to the clinical effects of sotatercept. The concurrent administration of sotatercept seems to correct the Activin A induced dysregulation of various genes associated with proliferation and apoptosis in both mutations.

The observed discrepancies between the two mutations concerning Activin stimulation and the effects of sotatercept on dysregulated genes related to proliferation and apoptosis may suggests an as yet unrecognized involvement of regulatory pathways beyond the canonical SMAD signaling.

These findings necessitate further comprehensive analyses, including the identification of principal regulators of proliferation and apoptosis in PAH, which may serve as novel therapeutic targets. Although the current study results do not definitively indicate whether sotatercept treatment can effectively reverse an already established Activin A-induced activation state of SMCs, the data nonetheless clearly recapitulate the known hallmarks of PAH and the therapeutic effects of sotatercept.

Next to hyperproliferation and resistance to apoptosis observed in vascular cells, increased vasoconstriction has been reported in PAH [60,61]. Pulmonary vascular dysfunction is present from the early stages of pathogenesis in pre-capillary arterioles, contributing to the end stage disease characterized by obliteration of the precapillary pulmonary arterioles [60]. The results of the conducted contraction assay also reflect the clinical PAH phenotype of increased vasoconstriction. iSMCs harboring both mutations exhibited a significantly increased contraction response compared to WT iSMCs upon Activin A stimulation. Although not reaching statistical significance, the observed elevated ratio of phosphorylated to non-phosphorylated myosin light chain (MLC) with Activin A stimulation further emphasizes the enhanced contractility of $BMPR2^{MutExDo}$ iSMCs in comparison to WT cells, whereas such an increase was not detectable in $BMPR2^{MutKiDo}$ iSMCs. This aligns with elevated pMLC levels in SMCs of some PAH patients [32]. While actin, another component of the contractile apparatus was significantly upregulated in iSMCs for both mutations, Activin A stimulation led to significant upregulation only in $BMPR2^{MutExDo}$ iSMCs in case of calponin 1. Supporting the findings of the contraction assay, pro-contractile genes are markedly upregulated in both $BMPR2^{Mut}$-iSMC types with Activin A treatment. However, whether the observed differences in the expression of individual genes and MLC phosphorylation indicate mutation-specific effects remains speculative at this stage.

Interestingly, sotatercept co-application largely reversed the mutation-dependent increase in contractility induced by Activin A treatment in $BMPR2^{MutExDo}$ iSMCs, and completely reversed it in $BMPR2^{MutKiDo}$ iSMCs. Furthermore, sotatercept application reduced the pMLC/MLC ratio

in Activin A stimulated BMPR2^{MutExDo} iSMCs to levels similar to those in BMPR2^{WT} cells.. Additionally, a significant decrease in the expression of actin and calponin 1 was observed in stimulated BMPR2^{MutExDo} iSMCs, consistent with previous observations in pulmonary artery smooth muscle cells derived from PAH-patients (PASMCs) [9]. This was accompanied by a reduced expression of pro-contractile genes in the BMPR2^{Mut} iSMCs with sotatercept. Together these findings suggest a hitherto unrecognized MoA of sotatercept, which may explain the rapid clinical response observed in a subgroup of patients, and which may operate synergistically with the known pro-apoptotic effects.

Another hallmark of PAH associated with pulmonary vascular remodeling is pathogenic deposition and composition of extracellular matrix in both distal and proximal pulmonary arteries [5]. Dysregulation of ECM assembly occurs early in the pathogenesis, leading to increased vessel wall thickness, the formation of occlusive intimal lesions, the loss of vascular elasticity, and heightened vessel stiffness [6]. While myofibroblasts appear during this process as the primary producers of ECM during development of PAH, it has been postulated that such cells may originate from local endothelial cells via EndoMT [41], or be derived from quiescent resident fibroblasts or bone marrow-derived circulating cells [39,40]. Since myofibroblasts are known to produce large quantities of collagen I during pathological tissue remodeling and fibrosis [62], we hypothesized that the cells producing high levels of collagen I under Activin A treatment of BMPR2^{Mut} iSMCs, may actually represent myofibroblasts formed from SMCs via the process of smooth muscle cell – to – myofibroblast transition (SMC-MFT). This process has been demonstrated experimentally in atherosclerosis [63], but the contribution of SMC-MFT has not yet been investigated in HPAH.

Contractile properties, collagen I production and appearance of the characteristic myofibroblasts features were more pronounced in Activin A-treated BMPR2^{MutExDo} iSMCs and less prominent in BMPR2^{MutKiDo} iSMCs. This finding potentially indicates differential effects on downstream signal transduction pathways. However, the increased expression of collagen I

and other genes associated with ECM formation, combined with the upregulation of genes characteristic of myofibroblasts and other mesenchymal cell types in Activin A-treated BMPR2^{Mut} iSMCs, clearly indicates a pathological transformation of BMPR2^{MutExDo} iSMCs into myofibroblasts. As our iSMC cultures consisted of highly enriched SMCs, and given that the upregulation of collagen I and actin filaments was observed in the vast majority of cells, it can be concluded that contaminating ECs or fibroblasts were not the source of the detected myofibroblasts. By contrast, the efficiency of myofibroblast formation following Activin A treatment suggests that SMC-MFT is the primary mechanism of myofibroblast formation in the arteries of PAH patients.

Notably, sotatercept treatment also significantly mitigated the effects of dysregulated ECM production and prevented the conversion of SMCs into myofibroblasts which may further contribute to the drug's anti-remodeling effects. Based on recently published data, we hypothesized that, in the myofibroblasts derived from our BMPR2^{Mut} iSMCs, mechanotransduction via ECM proteins and integrin complexes (ITGA/B) is creating a positive feedback loop [55] that promotes vascular remodeling in PAH [57]. Integrin α2 and β1 subunits form heterodimers that can bind to collagen I and serve as transmembrane receptors for outside-in signaling, thereby enabling mechanotransduction and stimulating TGFβ release and - signaling. Interestingly, we observed that sotatercept rescued the upregulation of the integrin subunit α2 as well as TGFβR1.

Following the integration of our findings into the existing understanding of PAH pathomechanisms, we propose a comprehensive model of PAH induction and pathogenesis (Fig. 5)[64].

In WT SMCs of the adjacent tunica media, Activin A and BMPs, particularly BMP9/10 via TGFβR1/ACTR2AB tetramers [65], and TGFβ through TGFβR1/TGFβR2, all contribute to the activation of TGFβ signaling via SMAD2/3. While the role of Activin A in activating the BMP pathway through SMAD1/5/9 can likely be disregarded due to its low affinity for ACVR1B/BMPR2 heterotetramers [66], BMPs effectively activate BMP signaling via

ACVRL1/BMPR2 or ACVR1/BMPR2 and SMAD1/5/9 [65], which in turn inhibits SMAD2/3 phosphorylation via SMAD6/7, thus limiting TGFβ signaling [67,68]. Moreover, BMPR2 acts as a gatekeeper to prevent the formation of high-affinity receptor complexes for TGFβ signaling [69]. These inhibitory mechanisms balance the positive feedback loop of the TGFβ pathway, which acts via an increased release of TGFβ from ECM stores mediated by mechanotransduction [57,69].

In PAH, the majority of BMPR2 mutations result in impaired or absent signal transduction by the BMPR1/BMPR2 complex, particularly with regard to the phosphorylation of SMAD1/5/9. Most mutations may mechanistically lead to an inability to bind the ligands, prevent receptor proteins from reaching the cell surface, cause mRNA degradation, or impair the kinase domain function [70-72]. Although not yet investigated, the mutations analyzed in our study most likely abrogate ligand binding and cell surface expression due to misfolding of the extracellular domain ($BMPR2^{MutExDo}$) or impair kinase activity ($BMPR2^{MutKiDo}$). Both of these lead to the abrogation of downstream SMAD1/5/9 phosphorylation. Additionally, mutations that lead to BMPR2 mRNA degradation or disturbed trafficking to the cell surface may result in increased formation of high-affinity receptor complexes for TGFβ signaling, consequently leading to enhanced SMAD2/3 phosphorylation [69].

Given that PAH-related *BMPR2* mutations are heterozygous, all downstream effects of these mutations will result solely in quantitative alterations to signaling pathways rather than complete abrogation. However, these quantitative shifts are apparently sufficient to cause minor pathological deviations that contribute to disease development in the long term.

While Activin A, BMPs, and TGFβ continue to activate SMAD2/3, the reduced phosphorylation of SMAD1/5/9 and SMAD6/7 leads to further increased phosphorylation of SMAD2/3. This dysregulates genes associated with proliferation, apoptosis inhibition, SMC contraction, transition into myofibroblasts, and ECM production, including collagen I. In addition, MLC is phosphorylated via activation of non-SMAD pathways. Consequently, mechanotransduction through the binding of collagen I to integrin receptors generates a positive feedback loop driven by the release of matrix-bound TGFβ1. This, in turn, further enhances SMAD2/3

phosphorylation and non-SMAD signaling, both of which stimulate pathological gene expression. Furthermore, an activation of predominantly non-SMAD by actin-myosin [73] and additionally by collagen-integrin-interactions [74] contributes to this positive feedback loop. The observed upregulation of the integrin receptor subunit α2 may further support this process. As a result, a self-sustaining imbalance between BMP and TGFβ signaling is induced, which reinforces the expression of Activin A [75-77], collagen, and actin–myosin components again [78,79], thereby driving the severe pathological progression in PAH [80].

Treatment with the Activin/BMP ligand trap sotatercept [13] appears to eliminate a significant portion – or at least a substantial part - of the available Activin A and BMP9/10 from serum and extracellular tissue fluids [81]. Apparently, despite the reduced phosphorylation of SMAD1/5/9 and the inhibitory SMADs 6/7, the attenuation of Activin A and BMP9/10 seems sufficient to downregulate the pathological feedback loop, which is otherwise sustained via binding of ECM-released TGFβ, Activin and BMP9/10. We hypothesize that decreased contractility and increased apoptosis in SMCs and SMC-derived myofibroblasts account for the rapid response to sotatercept in some patients, while the blockade of SMC-MFT and the reversal of the tissue remodeling leads to full therapeutic benefit.

Conclusion

We present the first PAH *in vitro* model based on patient iPSC-derived SMCs rather than iPSC-derived ECs. This model recapitulates key phenotypes of pulmonary vascular SMCs associated with PAH, including hyperproliferation, reduced apoptosis and dysregulated ECM deposition. It also revealed previously unrecognized cellular disease mechanisms, such as SMC-MFT, which leads to the accumulation of myofibroblasts and the aberrant deposition of extracellular matrix. Using this platform, we also investigated the mechanisms of action of the activin signaling inhibitor sotatercept. We confirmed its antiproliferative and proapoptotic effects and demonstrated inhibition of smooth muscle cell contractility and SMC-MFT, which likely contribute to its therapeutic effects.

455

Figure legends

Figure 1: BMPR2^{Mut}iSMCs exhibit increased proliferation and decreased apoptosis, hallmarks of PAH, and recapitulate clinical drug responsiveness in vitro. (**A**) Schematic illustration of chemically defined differentiation protocol from iPSCs to iSMCs. (**B**) Differentiation efficacy determined by flow cytometric analysis of CD140b positive cells. (Data is presented as mean ± SD). (**C**) Immunofluorescence analysis for SMC markers confirms SMC identity of iSMCs (alpha-smooth muscle actin (Actin) and calponin (CNN1) (both green), myosin heavy chain 11 (MHY11) (red), nuclei (DAPI, blue), scale bar 200 µm. (**D**) SMC score calculated as the mean expression of Travaglini SMC genes (MSigDB: M41672) in human pulmonary artery smooth muscle cells (GSE144274), human iPSC lines (HipSci resource) and merged expression values of untreated iSMCs from all lines and clones. (**E**) PCA analysis of untreated iSMCs based on 2000 most variable genes (Log2(TPM+1)) of three independent WT cell lines (dark green dots) and three clones per BMPR2-mutant of, whereas BMPR2^{MutExDo} (light green dots) and BMPR2^{MutKiDo} (medium green dots); average of each experimental groups depicted as cross. (**F**) Quantification of cell numbers relative to the respective vehicle control after 8d treatment. Data is presented as mean ± SD, n= 3 independent biological replicates per column indicated as dots. Exploratory two-way ANOVA with genotype and treatment as factors was followed by Sidak´s multiple-comparisons test to compare genotype differences within Activin A treatment and to compare effects of Activin A, and Activin A in combination with sotatercept, within each genotype. ns, not significant; *p < 0.05, **p < 0.01, ***p < 0.001. (**G**) Quantification of apoptotic signal measured as caspase3/7 activity and normalization to respective cell number after 5d treatment. Data is presented as mean ± SD, n= 6-9 independent biological replicates per column indicated as dots. Two-way ANOVA with genotype and treatment as factors was followed by Sidak´s multiple-comparisons test to compare genotype differences within Activin A treatment and to compare effects of Activin A and Activin A in combination with sotatercept within each genotype. ns, not significant; *p < 0.05, **p < 0.01, ***p < 0.001.

Figure 2: Inhibition of Activin A-induced SMC contraction by sotatercept. (**A**) Functional contraction assay with iSMCs derived from representative WT cell line or BMPR2^{Mut} clones. Double arrow indicates well diameter as starting position for contraction. (**B**) Contraction was determined as the area of the gel disc after 72 h relative to the initial area of the iSMC-gel-discs. Data is presented as mean ± SD, n= 3 independent biological replicates per column indicated as dots. Exploratory two-way ANOVA with genotype and treatment as factors was followed by Sidak´s multiple-comparisons test to compare genotype differences within Activin A treatment and to compare effects of Activin A and Activin A in combination with sotatercept within each genotype. ns, not significant; *p < 0.05, **p < 0.01, ***p < 0.001. (**C**)

Quantification of the ratio of phosphorylated myosin light chain (pMLC) to total MLC by automated capillary-based western blot analysis. Data is presented as mean ± SD, n= 3 independent biological replicates per column indicated as dots. Exploratory two-way ANOVA with Sidak´s multiple-comparisons was used to compare genotype differences within Activin A or Activin A in combination with sotatercept, followed by two-tailed unpaired Student's t-tests for treatment comparisons within each genotype. ns, not significant; *p < 0.05, **p < 0.01, ***p < 0.001. (**D, F**) Immunofluorescence staining of components of the contractile apparatus in iSMCs of one iPSC line / clone representative for the respective genotype ($BMPR2^{WT}$, $BMPR2^{MutExDo}$, $BMPR2^{MutKiDo}$). Actin and calponin (CNN1) (green), nuclei DAPI (blue), scale bar 200 µm. (**E**) Quantification of actin from immunofluorescence images expressed as mean fluorescence intensity (MFI) normalized to cell number (DAPI). Data is presented as mean ± SD, n= 6 independent biological replicates per column indicated as dots. Two-way ANOVA with genotype and treatment as factors was followed by Sidak´s multiple-comparisons test to compare genotype differences within Activin A treatment and to compare effects of Activin A and Activin A in combination with sotatercept within each genotype. ns, not significant; *p < 0.05, **p < 0.01, ***p < 0.001. (**G**) Quantification of CNN1 from flow cytometry analysis (MFI). Data is presented as mean ± SD, n= 3 independent biological replicates per column indicated as dots. Exploratory two-way ANOVA with genotype and treatment as factors was followed by Sidak´s multiple-comparisons test to compare genotype differences within Activin A treatment and to compare effects of Activin A and Activin A in combination with sotatercept within each genotype. ns, not significant; *p < 0.05, **p < 0.01, ***p < 0.001. (**H**) Heatmaps showing differentially expressed genes with pro-contractile function in Activin A vs. Activin A + sotatercept treated iSMCs each condition normalized to the untreated control. For contraction gene set scoring (MSigDB: M1429), bulk RNA-seq expression values were analysed using a gene-by-sample FPKM matrix (mean FPKM of three independent biological replicates per group, Activin A and Activin A + sotatercept). Stars (*) highlight mentioned genes in the respective text.

Figure 3: SMC-to-Myofibroblast transition (SMC-MFT) contributes to arterial tissue remodeling in PAH. (**A**) Immunofluorescence staining of iSMCs from one iPSC line/clone representative for the respective genotype ($BMPR2^{WT}$, $BMPR2^{MutExDo}$, $BMPR2^{MutKiDo}$) for collagen I (orange) and actin (green), nuclei DAPI (blue), scale bar 200 µm. (**B**) Quantification of collagen I content per cell normalized to untreated control by siriusRed assay. Data is presented as mean ± SD, n= 4-7 independent biological replicates per column indicated as dots. Exploratory two-way ANOVA with genotype and treatment as factors was followed by Sidak´s multiple-comparisons test to compare genotype differences within Activin A treatment and to compare effects of Activin A and Activin A in combination with sotatercept within each genotype. ns, not significant; *p < 0.05, **p < 0.01, ***p < 0.001. (**C**) Heatmaps showing

differentially expressed genes associated with extracellular matrix production in Activin A vs. Activin A + sotatercept treated iSMCs each condition normalized to the untreated control. For ECM gene set scoring (MSigDB: M11366), bulk RNAseq expression values were analyzed using a gene-by-sample FPKM matrix (mean FPKM of three independent biological replicates per group, Activin A and Activin A + sotatercept). Stars (*) highlight mentioned genes in the respective text. (**D**) Functional enrichment analysis of positive regulated genes from the gene set enrichment analysis from iSMCs bulk RNAseq with Enrichr [82]. Bar plot shows enriched cell types from CellMarker 2024. Bar length represents significance of enrichment. (**E**) Myofibroblast signature score from the bulk RNA-seq FPKM expression matrix using a predefined, manually curated set of myofibroblast-associated marker genes, top 100 genes of three independently annotated human lung single-cell RNAseq datasets: GSE135893, GSE136831 and the Munich cohort dataset from Mayr et al, 2021. Boxes indicate the interquartile range (25th–75th percentile), the center line denotes the median, and whiskers extend to 1.5 × the interquartile range. Each point represents an individual biological sample. (**F**) Heatmaps showing differentially expressed pro-myofibroblast genes in Activin A vs. Activin A + sotatercept treated iSMCs each condition normalized to the untreated control. For myofibroblast gene set scoring, bulk RNAseq expression values were analysed using a gene-by-sample FPKM matrix (mean FPKM of three independent biological replicates per group, Activin A and Activin A + sotatercept). Stars (*) highlight mentioned genes in the respective text.

Figure 4: Activin A induces a pathological upregulation of collagen-integrin mechano-signaling and TGFβ-signaling in BMPR2^{MutExDo} iSMCs. (**A**) TGFβ content in patient sera at baseline and on sotatercept treatment determined by ELISA (on-treatment samples obtained 9–41 months after sotatercept initiation). Each dot represents an individual patient (n=8), with lines connecting paired pre-and on-sotatercept. Horizontal lines indicate mean. Statistical significance was assessed using a two-tailed Wilcoxon matched-pairs sign-rank test. ns, not significant; *p < 0.05, **p < 0.01, ***p < 0.001. (**B**) Immunofluorescence staining of iSMCs from one line/clone representative for the respective genotype (BMPR2^{WT}, BMPR2^{MutExDo}, BMPR2^{MutKiDo}) stained for integrin-α2 (ITGA2, orange), actin (green), nuclei DAPI (blue), scale bar 200 µm. (**C**) Quantification of ITGA2 in iSMCs via flow cytometry (MFI). Data is presented as mean ± SD, n= 3 independent biological replicates per column indicated as dots. Exploratory two-way ANOVA with genotype and treatment as factors was followed by Sidak´s multiple-comparisons test to compare genotype differences within Activin A treatment and to compare effects of Activin A and Activin A in combination with sotatercept within each genotype. ns, not significant; *p < 0.05, **p < 0.01, ***p < 0.001. (**D**) Immunofluorescence staining of iSMCs derived from one iPSC line / clone representative for the respective genotype (BMPR2^{WT}, BMPR2^{MutExDo}, BMPR2^{MutKiDo}) for TGFβR1 (orange) and calponin (CCN1, green)

nuclei DAPI (blue), scale bar 200 µm. (**E**) Quantification of TGFβR1 in iSMCs via flow cytometry (MFI). Data is presented as mean ± SD, n= 3 independent biological replicates per column indicated as dots. Exploratory two-way ANOVA with genotype and treatment as factors was followed by Sidak´s multiple-comparisons test to compare genotype differences within Activin A treatment and to compare effects of Activin A and Activin A in combination with sotatercept within each genotype. ns, not significant; *p < 0.05, **p < 0.01, ***p < 0.001.

Figure 5: Schematic illustration of the hypothesized maladaptive Activin A/TGFβ signaling axis in crosstalk with the collagen I-integrin signaling leading to a pathological feedback loop, triggering smooth muscle cell–to–myofibroblast transition (SMC-MFT) in BMPR2^{Mut}-iSMCs. Created in BioRender. Olmer, R. (2026) https://BioRender.com/d3lee4y

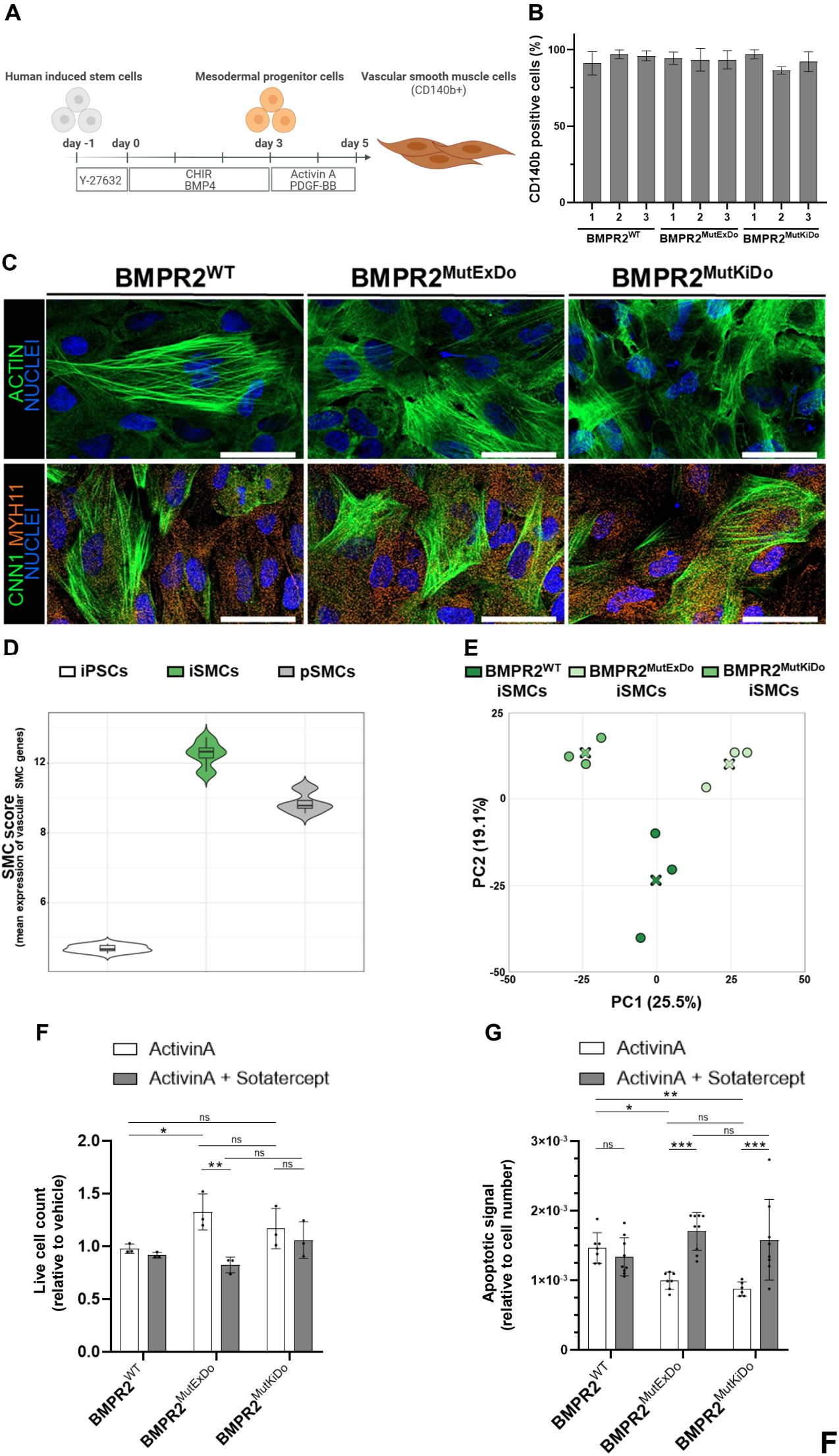
A
Human induced stem cells
Mesodermal progenitor cells
Vascular smooth muscle cells
(CD140b+)
day -1
day 0
day 3
day 5
Y-27632
CHIR
BMP4
Activin A
PDGF-BB
B
CD140b positive cells (%)
100
50
0
1 2 3 1 2 3 1 2 3
BMPR2WT
BMPR2MutExDo
BMPR2MutKiDo
C
BMPR2WT
BMPR2MutExDo
BMPR2MutKiDo
ACTIN
NUCLEI
CNN1 MYH11
NUCLEI
D
iPSCs
iSMCs
pSMCs
SMC score
(mean expression of vascular SMC genes)
12
8
6
E
BMPR2WT iSMCs
BMPR2MutExDo iSMCs
BMPR2MutKiDo iSMCs
PC2 (19.1%)
PC1 (25.5%)
25
0
-25
-50
-50
-25
0
25
50
F
ActivinA
ActivinA + Sotatercept
Live cell count
(relative to vehicle)
2.0
1.5
1.0
0.5
0.0
ns
*
ns
**
ns
ns
BMPR2WT
BMPR2MutExDo
BMPR2MutKiDo
G
ActivinA
ActivinA + Sotatercept
Apoptotic signal
(relative to cell number)
3×10-3
2×10-3
1×10-3
0
**
*
ns
ns
ns
***
***
BMPR2WT
BMPR2MutExDo
BMPR2MutKiDo

Figure 1

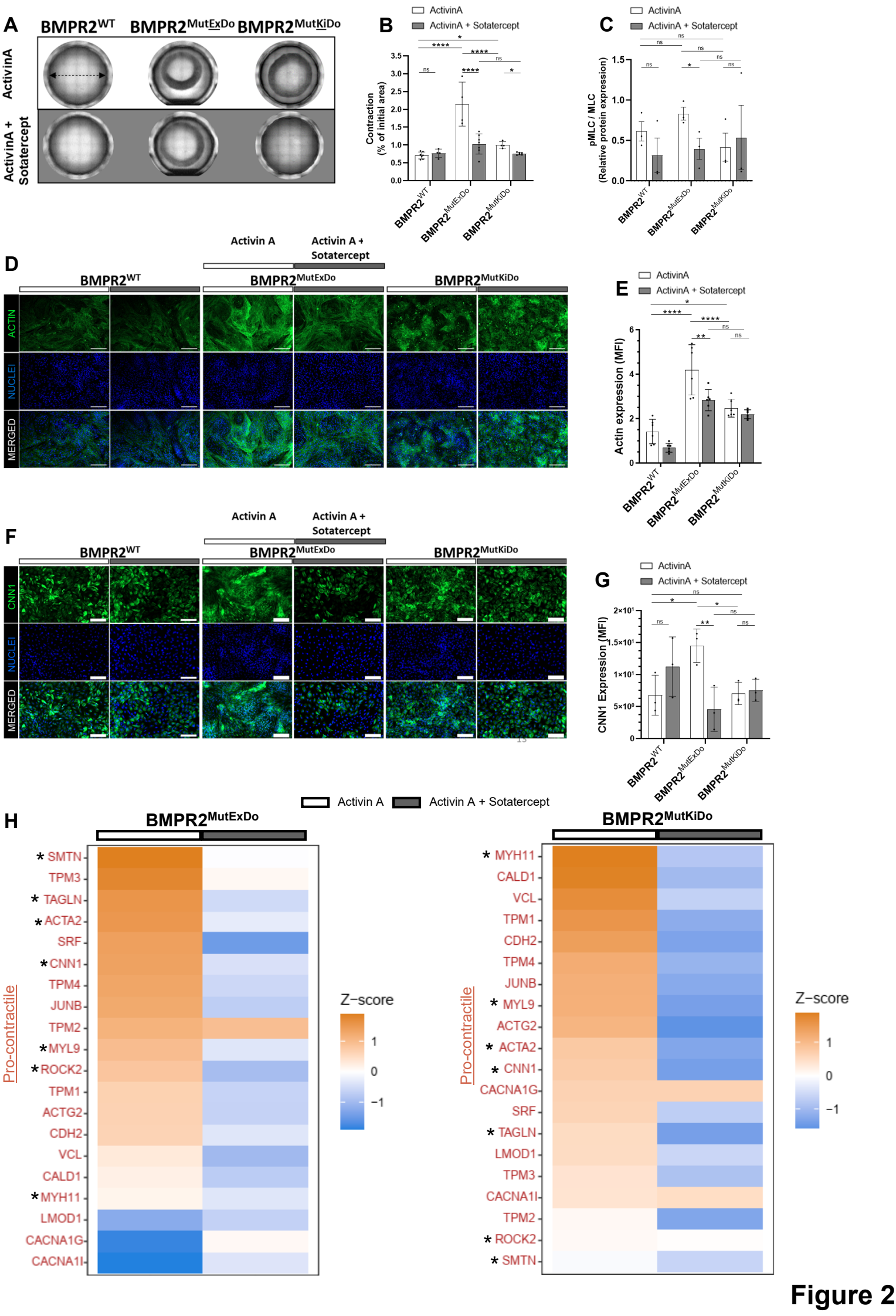
A
BMPR2WT
BMPR2MutExDo
BMPR2MutKiDo
ActivinA
ActivinA + Sotatercept
B
ActivinA
ActivinA + Sotatercept
Contraction (% of initial area)
BMPR2WT
BMPR2MutExDo
BMPR2MutKiDo
C
ActivinA
ActivinA + Sotatercept
pMLC / MLC (Relative protein expression)
D
Activin A
Activin A + Sotatercept
BMPR2WT
BMPR2MutExDo
BMPR2MutKiDo
ACTIN
NUCLEI
MERGED
E
ActivinA
ActivinA + Sotatercept
Actin expression (MFI)
F
Activin A
Activin A + Sotatercept
CNN1
NUCLEI
MERGED
G
ActivinA
ActivinA + Sotatercept
CNN1 Expression (MFI)
Activin A
Activin A + Sotatercept
H
BMPR2MutExDo
BMPR2MutKiDo
Pro-contractile
SMTN
TPM3
TAGLN
ACTA2
SRF
CNN1
TPM4
JUNB
TPM2
MYL9
ROCK2
TPM1
ACTG2
CDH2
VCL
CALD1
MYH11
LMOD1
CACNA1G
CACNA1I
Z−score
MYH11
CALD1
VCL
TPM1
CDH2
TPM4
JUNB
MYL9
ACTG2
ACTA2
CNN1
CACNA1G
SRF
TAGLN
LMOD1
TPM3
CACNA1I
TPM2
ROCK2
SMTN

Figure 2

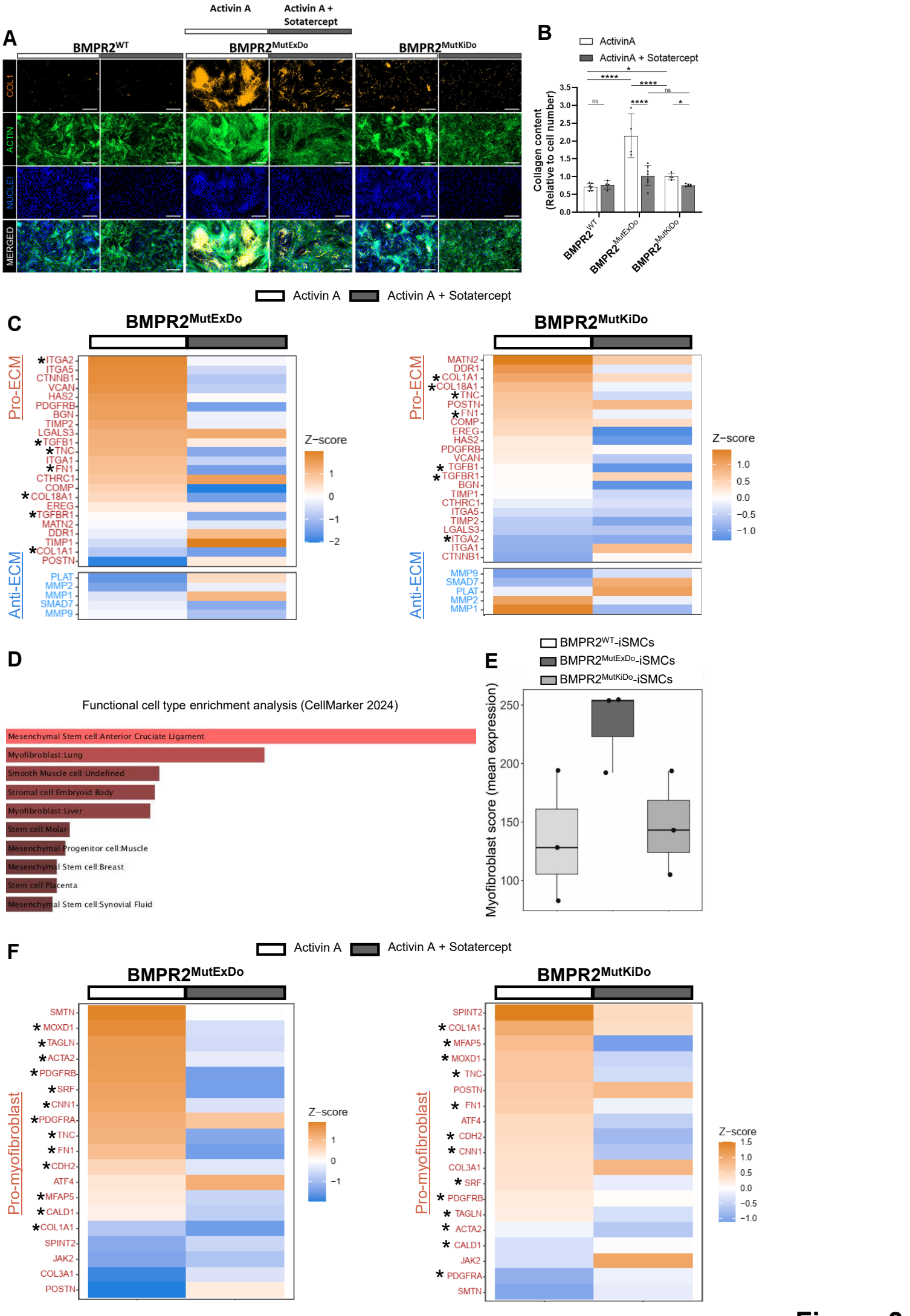
A
Activin A
Activin A + Sotatercept
BMPR2WT
BMPR2MutExDo
BMPR2MutKiDo
COL1
ACTIN
NUCLEI
MERGED
B
ActivinA
ActivinA + Sotatercept
Collagen content (Relative to cell number)
ns
****
*
Activin A
Activin A + Sotatercept
C
BMPR2MutExDo
BMPR2MutKiDo
Pro-ECM
Anti-ECM
ITGA2
ITGA5
CTNNB1
VCAN
HAS2
PDGFRB
BGN
TIMP2
LGALS3
TGFB1
TNC
ITGA1
FN1
CTHRC1
COMP
COL18A1
EREG
TGFBR1
MATN2
DDR1
TIMP1
COL1A1
POSTN
PLAT
MMP2
MMP1
SMAD7
MMP9
Z−score
D
Functional cell type enrichment analysis (CellMarker 2024)
Mesenchymal Stem cell:Anterior Cruciate Ligament
Myofibroblast:Lung
Smooth Muscle cell:Undefined
Stromal cell:Embryoid Body
Myofibroblast:Liver
Stem cell:Molar
Mesenchymal Progenitor cell:Muscle
Mesenchymal Stem cell:Breast
Stem cell:Placenta
Mesenchymal Stem cell:Synovial Fluid
E
BMPR2WT-iSMCs
BMPR2MutExDo-iSMCs
BMPR2MutKiDo-iSMCs
Myofibroblast score (mean expression)
F
Activin A
Activin A + Sotatercept
BMPR2MutExDo
BMPR2MutKiDo
Pro-myofibroblast
SMTN
MOXD1
TAGLN
ACTA2
PDGFRB
SRF
CNN1
PDGFRA
TNC
FN1
CDH2
ATF4
MFAP5
CALD1
COL1A1
SPINT2
JAK2
COL3A1
POSTN
Z−score

Figure 3

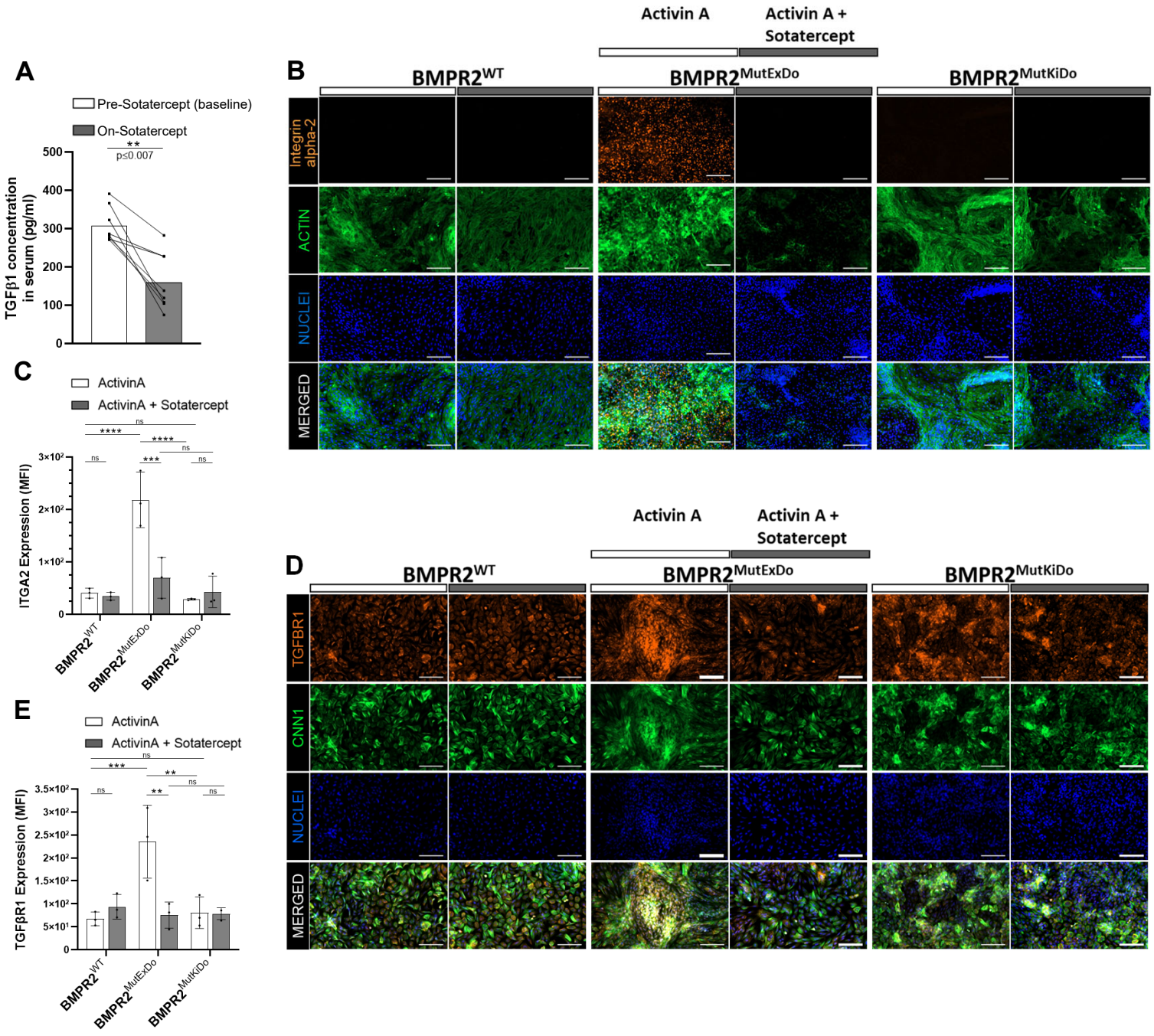
A
Pre-Sotatercept (baseline)
On-Sotatercept
**
p≤0.007
TGFβ1 concentration in serum (pg/ml)
500
400
300
200
100
0
B
Activin A
Activin A + Sotatercept
BMPR2WT
BMPR2MutExDo
BMPR2MutKiDo
Integrin alpha-2
ACTIN
NUCLEI
MERGED
C
ActivinA
ActivinA + Sotatercept
ITGA2 Expression (MFI)
3×10²
2×10²
1×10²
0
ns
****
***
BMPR2WT
BMPR2MutExDo
BMPR2MutKiDo
D
Activin A
Activin A + Sotatercept
BMPR2WT
BMPR2MutExDo
BMPR2MutKiDo
TGFBR1
CNN1
NUCLEI
MERGED
E
ActivinA
ActivinA + Sotatercept
TGFβR1 Expression (MFI)
3.5×10²
3×10²
2.5×10²
2×10²
1.5×10²
1×10²
5×10¹
0
***
**
ns
BMPR2WT
BMPR2MutExDo
BMPR2MutKiDo

Figure 4

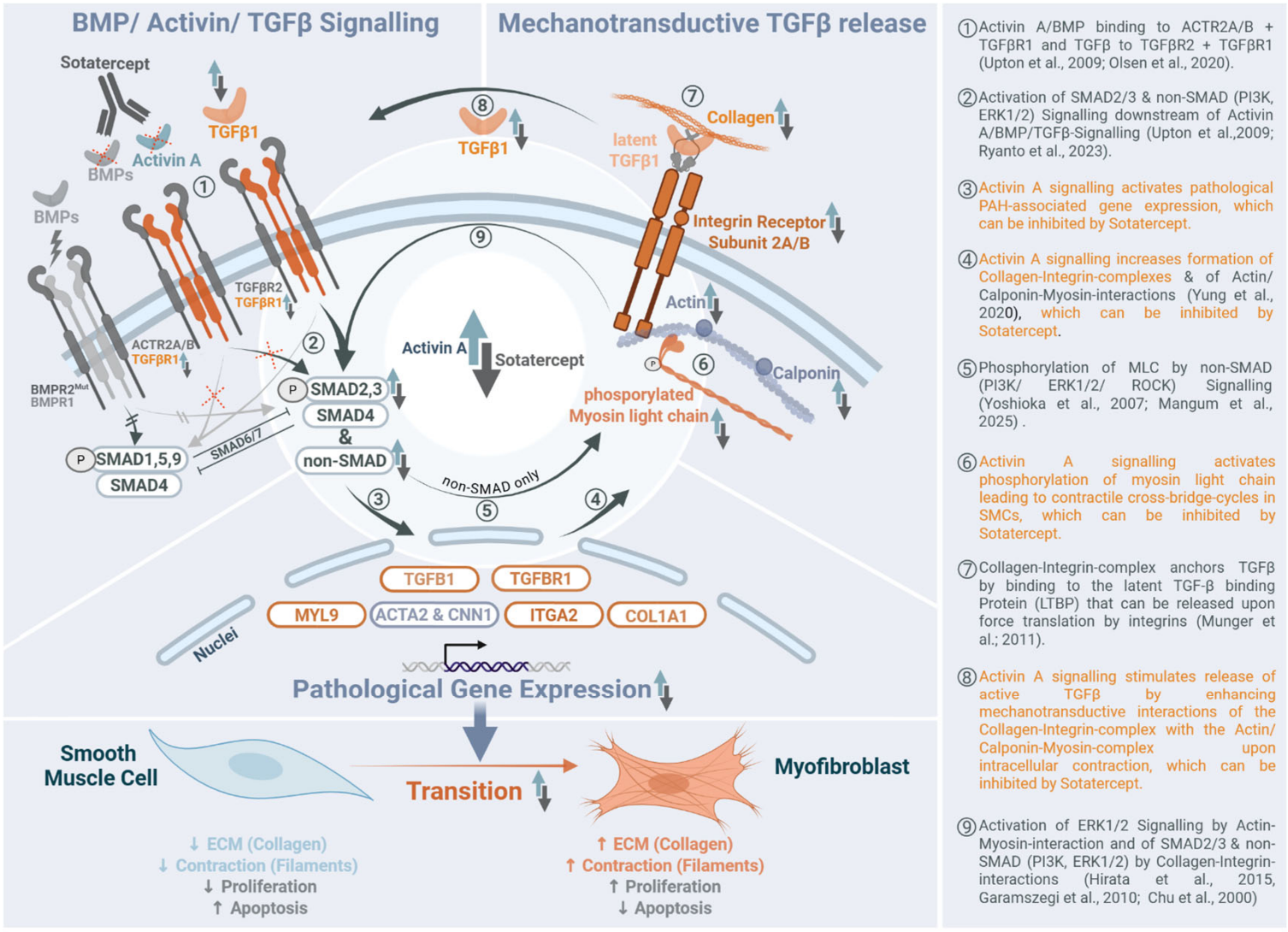

① Activin A/BMP binding to ACTR2A/B + TGFβR1 and TGFβ to TGFβR2 + TGFβR1 (Upton et al., 2009; Olsen et al., 2020).

② Activation of SMAD2/3 & non-SMAD (PI3K, ERK1/2) Signalling downstream of Activin A/BMP/TGFβ-Signalling (Upton et al.,2009; Ryanto et al., 2023).

③ Activin A signalling activates pathological PAH-associated gene expression, which can be inhibited by Sotatercept.

④ Activin A signalling increases formation of Collagen-Integrin-complexes & of Actin/ Calponin-Myosin-interactions (Yung et al., 2020), which can be inhibited by Sotatercept.

⑤ Phosphorylation of MLC by non-SMAD (PI3K/ ERK1/2/ ROCK) Signalling (Yoshioka et al., 2007; Mangum et al., 2025) .

⑥ Activin A signalling activates phosphorylation of myosin light chain leading to contractile cross-bridge-cycles in SMCs, which can be inhibited by Sotatercept.

⑦ Collagen-Integrin-complex anchors TGFβ by binding to the latent TGF-β binding Protein (LTBP) that can be released upon force translation by integrins (Munger et al.; 2011).

⑧ Activin A signalling stimulates release of active TGFβ by enhancing mechanotransductive interactions of the Collagen-Integrin-complex with the Actin/ Calponin-Myosin-complex upon intracellular contraction, which can be inhibited by Sotatercept.

⑨ Activation of ERK1/2 Signalling by Actin-Myosin-interaction and of SMAD2/3 & non-SMAD (PI3K, ERK1/2) by Collagen-Integrin-interactions (Hirata et al., 2015, Garamszegi et al., 2010; Chu et al., 2000)

Smooth muscle cell-to-myofibroblast transition in HPAH and inhibition by Sotatercept. Orange color indicates novelty in terms of stimulation by activin A and/or inhibition by Sotatercept (see text on the right for details). Blue arrows display upregulation of the intermediate/process by activin A; dark grey arrows indicate downregulation of the intermediate/process by Sotatercept in iSMCs. Lightning symbol illustrates deficient BMPR2 signalling due to BMPR2 mutation. Red crosses indicate inhibited activin/BMP signalling in the presence of Sotatercept. Black arrows represent primary dominant signalling; light grey arrows show alternative signalling.

Figure 5

Supplementary Figure legends

Supplementary figure 1: Sotatercept leads to upregulation of antiproliferative genes in Activin A-treated BMPR2^{mutExDo} iSMCs.

Heatmaps showing differentially expressed genes associated with proliferation in Activin A vs. Activin A + sotatercept treated iSMCs. For proliferation gene set (MSigDB: M16210) scoring, bulk RNAseq expression values were analyzed using a gene-by-sample FPKM matrix (mean FPKM of three independent biological replicates per group, Activin A and Activin A + sotatercept each condition normalized to the untreated control). Stars (*) highlight mentioned genes in the respective text.

Supplementary figure 2: Sotatercept leads to upregulation of antiproliferative genes in Activin A-treated BMPR2^{mutExDo} iSMCs.

Heatmaps showing differentially expressed genes associated with apoptosis in Activin A vs. Activin A + sotatercept treated iSMCs. For apoptosis gene set (MSigDB: M5902) scoring, bulk RNA-seq expression values were analyzed using a gene-by-sample FPKM matrix (mean FPKM of three independent biological replicates per group, Activin A and Activin A + sotatercept each condition normalized to the untreated control). Stars (*) highlight mentioned genes in the respective text.

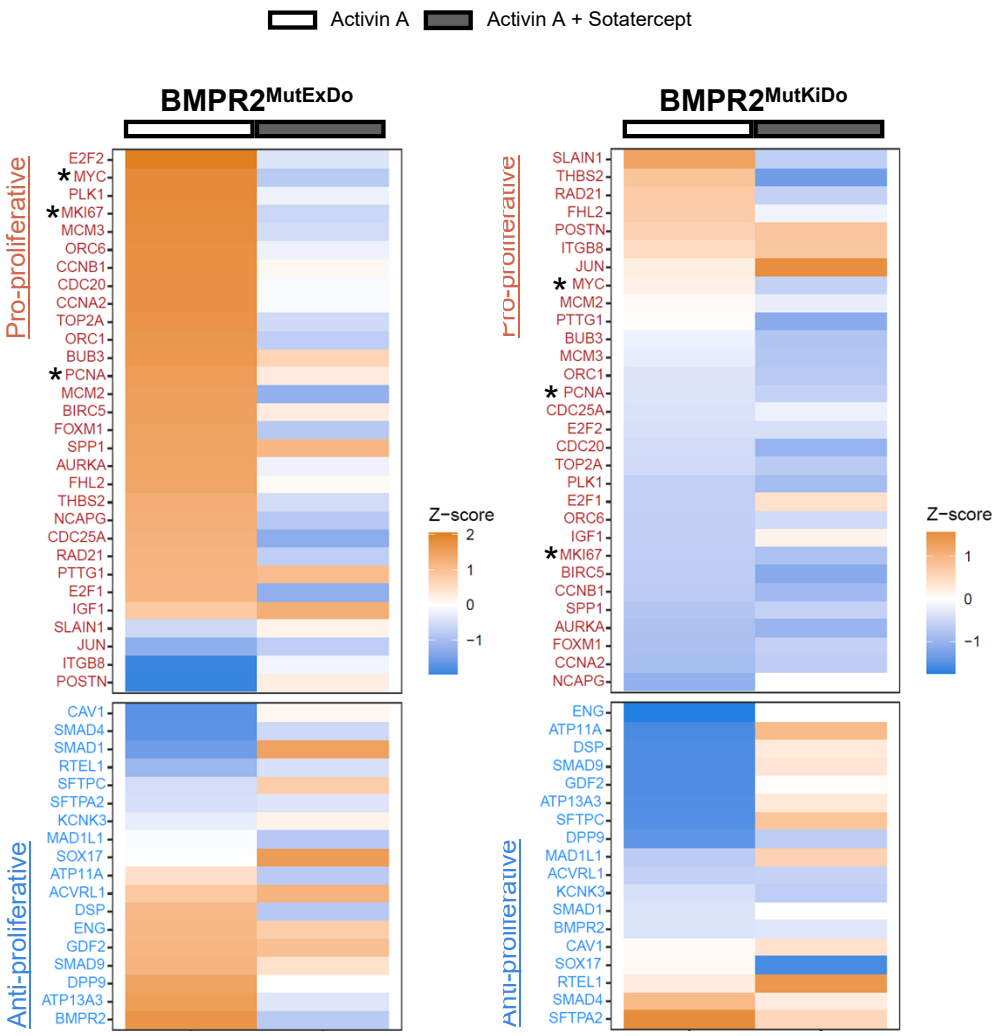

Supplementary Figure 1

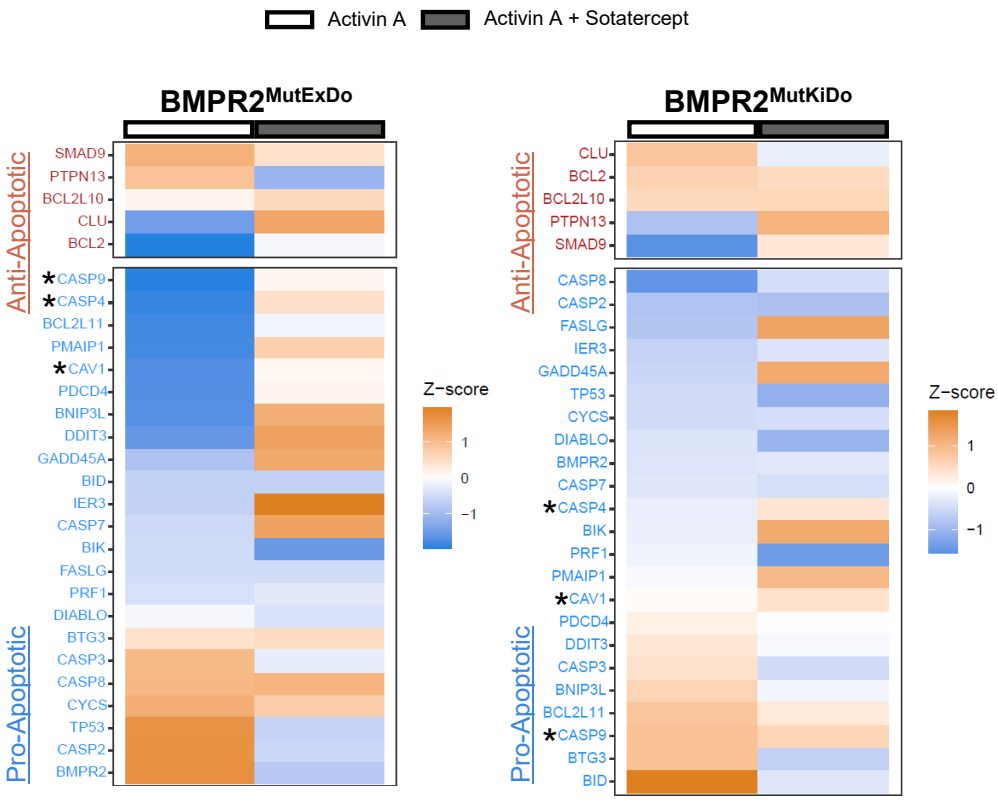

Supplementary Figure 2

Material and Methods

Human subjects

This study is an exploratory analysis to translate the results from the HPAH iSMC *in vitro* model to HPAH patients, to offer further insights into the therapeutic response to sotatercept in patients. For a paired analysis, TGFβ content in patient sera at baseline and on sotatercept treatment was examined from eight patients and on-treatment samples were obtained 9–41 months after sotatercept initiation. All patients signed the German Centre for Lung Research informed consent form (https://dzl.de/en/dzl-data-warehouse), which permits the use of clinical routine data and blood samples for research purposes. This form has been approved by our institution's ethics committee (number 8540_BO_K_ 2019)."

Sample collection and processing

Peripheral blood samples were taken from the same patients before and during therapy with sotatercept. Samples were collected in serum tubes, allowed to clot, processed within 2 h, and centrifuged at 1,500 g for 10 min at 4 °C. Serum was aliquoted and stored at -80 °C until ELISA analysis.

ELISA-human TGFβ1 (Transforming growth factor beta-1)

Human transforming growth factor beta-1 (TGFβ1) was quantified in serum samples from HPAH patients by ELISA (Abcam, cat. no. ab100647). Latent TGFβ1 was activated by incubating 50 µL of 1 N HCL with 100 µL serum (FCS; PAN Biotech, cat. no. P30-3306) for 10 min at room temperature (RT). The acidified serum was neutralized by adding 50 µL of 1.2 N NaOH/0.5 M HEPES and assayed immediately. The sandwich ELISA was performed as follows: 100 µL of standard and sample was incubated overnight (ON) at 4°C with gentle shaking. The next day, wells were washed four times with 300 µL of the washing solution and plate was blotted against clean paper towels. In the next step, 100 µL of the 1x biotinylated TGFβ1 detection antibody per well was added and incubated for 1 h at RT with gentle shaking. Wells were washed again. Then, 100 µL of 1x HRP-streptavidin solution was added and incubated for 45 min at RT with gentle shaking. Wells were washed again and 100 µL of the TMB one-step substrate reagent was added and incubated for 30 min at RT in the dark with gentle shaking. Finally, 50 µL of the stop solution was added to each well and absorbance was measured at 450 nm.

Human induced pluripotent stem cells (hiPSCs)

For HPAH *in vitro* modelling, three iPSC clones per patient cell line were compared to three independent cell lines from healthy individuals. The following human pluripotent stem cell lines were generated from $CD34^{pos}$ cells using the CytoTune®-iPS 2.0 Sendai Reprogramming Kit (Thermo Fisher Scientific, cat. no. 16517), following the manufacturer's instructions: WT1 (MHHi001-A; clone 2; male), WT2 (MHHi038-A; clone 20; male), WT3 (MHHi039-A clone 12; female), $BMPR2^{MutExDo}$ heterozygous in-frame-deletion c.248-1 – 418+1 of exon 3 in the extracellular domain, (MHHi023-A; clone 18, 25, 26; female), $BMPR2^{MutKiDo}$ (heterozygous missense mutation c.1471C>T in exon 11 in the kinase domain), MHHi024-A; clone 14, 16, 18; female). Pluripotency and genomic stability were tested for all hiPSC lines (Usman et al., 2021). Informed consent for blood collection, iPSC generation and anonymous data storage was obtained from the patients or legal caregivers according to the principles expressed in the Declaration of Helsinki (pediatric IRB approval #2200 to G.H., Hannover Medical School; 2926-2015). hiPSCs were maintained on vitronectin-coated (Gibco, cat. no. A31804) plates (Nunc, cat. no. 140675) in Essential 8 medium (DMEM/F12 (ThermoFisher, cat. no. 11330-057), 64 mg/L ascorbic acid 2-phosphate (Sigma-Aldrich, cat. no. A92902), 14 µg/L sodium selenite (Sigma-Aldrich, cat. no. 214485), 543 mg/L sodium bicarbonate (Sigma Aldrich, cat. No. 55761), 20 µg/L Insulin (Sigma-Aldrich, cat. no. I9278), 10.7 µg/mL human recombinant transferrin (Sigma-Aldrich, cat. no. T3705), 100 ng/mL bFGF (Peprotech, cat. no. AF-100-18B), 2 ng/mL TGFb1 (PeproTech, cat. no. 100-21C)). Cells were passaged every 3–4 days using Accutase™ (Gibco, cat. no. A1110501) at 32,000 cells/cm^2 and cultivated at 37 °C, 5% CO2. Cells were tested monthly for mycoplasma contamination using the MycoStrip® - Mycoplasma Detection Kit (Invivogen, cat. no. REP-MYS). Passages between 4 to 8 were used for starting directed differentiation into vascular smooth muscle cells.

Differentiation in iPSC-derived smooth muscle cells (iSMCs)

Differentiation of iPSCs into vascular smooth muscle cells (iSMCs) was performed following a modified protocol derived from (Patsch et. al, 2015), described in detail below. On day 0, iPSCs were seeded at 12,000 cells/cm² and cultivated in Essential 8 medium (DMEM/F12 (ThermoFisher, cat. no. 11330-057), 64 mg/L ascorbic acid 2-phosphate (Sigma-Aldrich, cat. no. A92902), 14 µg/L sodium selenite (Sigma-Aldrich, cat. no. 214485), 543 mg/L sodium bicarbonate (Sigma Aldrich, cat. No. 55761), 20 µg/L Insulin (Sigma-Aldrich, cat. no. I9278), 10.7 µg/mL human recombinant transferrin (Sigma-Aldrich, cat. no. T3705), 100 ng/mL bFGF (Peprotech, cat. no. AF-100-18B), 2 ng/mL TGFb1 (PeproTech, cat. no. 100-21C)) with 10 µM Y-27632 (Tocris, cat. no. 1254) for 24 h. On day 1, medium was changed to Essential 6 medium (DMEM/F12 (ThermoFisher, cat. no. 11330-057), 64 mg/L ascorbic acid 2-phosphate (Sigma-Aldrich, cat. no. A92902), 14 µg/L sodium selenite (Sigma-Aldrich, cat. no. 214485), 543 mg/L sodium bicarbonate (Sigma Aldrich, cat. No. 55761), 20 µg/L Insulin (Sigma-Aldrich,

cat. no. I9278), 10.7 µg/mL human recombinant transferrin (Sigma-Aldrich, cat. no. T3705) supplemented with 7.5 µM CHIR66021 (provided by the Institute of Organic Chemistry, Leibniz University, Hannover, Germany) and 25 ng/mL BMP4 (R&D Systems, cat. no. 314-BP) for mesoderm induction via Wnt modulation. On day 4, medium was replaced by Essential 6 medium supplemented with 2 ng/mL Activin A (Peprotech, cat. no. 120-14E) and 10 ng/mL PDGF-BB (Peprotech, cat. no. 100-14B) for vascular SMC specification. On day 6, the differentiation process was terminated by dissociating and seeding the cells on different formats for further analysis. The differentiation efficiency and therefore purity of generated iSMCs was assessed via CD140b in flow cytometry.

Flow cytometric analysis

Flow analysis was used for detection of surface and intracellular markers of iSMCs. For assessing the differentiation efficacy, freshly differentiated iSMCs were stained with directly labeled CD140b-APC (APC, Miltenyi Biotec, cat. no. 130-121-052, RRID:AB_2783952, recombinant human, 1:50) in PBS pH7.4 (1X) (Gibco, cat. no. 70011-036) supplemented with 1 % FCS (PAN Biotech, cat. no. P30-3306) and 1 mM EDTA (Sigma Aldrich, cat. no. E5134) for 45 min and propidium iodide (Miltenyi Biotec, cat. no. 130-093-233, 1:100) for 5 min, to exclude dead cells. For the quantification of HPAH phenotypic markers, freshly differentiated iSMCs were seeded as passage 1 at 20.000 cells/cm^2 on vitronectin-coated (Gibco, cat. no. A31804) plates (Nunc, cat. no. 140675) in 200 µL/cm^2 Essential 6 (DMEM/F12 (ThermoFisher, cat. no. 11330-057), 64 mg/L ascorbic acid 2-phosphate (Sigma-Aldrich, cat. no. A92902), 14 µg/L sodium selenite (Sigma-Aldrich, cat. no. 214485), 543 mg/L sodium bicarbonate (Sigma Aldrich, cat. No. 55761), 20 µg/L Insulin (Sigma-Aldrich, cat. no. I9278), 10.7 µg/mL human recombinant transferrin (Sigma-Aldrich, cat. no. T3705) with 10 µM Y-27632 (Tocris, cat. no. 1254) and cultivated at 37°C and 5% CO_2 for 24 h. Between day 1-12, every 48 h media was changed to 200 µL/cm^2 E6 with additives of Activin A (Peprotech, cat. no. GMP120-14E, 0.25 ng/ml), sotatercept (MedChemExpress, HY-P99590, 10 µg/ml) or Activin A with sotatercept. On day 12, for the quantification of HPAH phenotypic surface markers cells were fixed with 4% paraformaldehyde (Sigma-Aldrich, cat. no.158127) for 10 min, with ice-cold 90% methanol (JT Baker, cat. no. 8045) for 15 min and stained with a primary antibody for TGFβR1 (Thermo Fisher Scientific, cat. no. PA5-142789, RRID:AB_2933432, rabbit, 1:100) in PBS pH7.4 (1X) (Gibco, cat. no. 70011-036) supplemented with 1 % FCS (PAN Biotech, cat. no. P30-3306) and 1 mM EDTA (Sigma Aldrich, cat. no. E5134) over night at 4 °C. Cells were stained with a secondary antibody anti-rabbit (Cy5, Jackson ImmunoResearch Labs, cat. no. 711-175-152, RRID:AB_2340607, donkey, 1:300) in PBS pH7.4 (1X) (Gibco, cat. no. 70011-036) supplemented with 1 % FCS (PAN Biotech, cat. no. P30-3306) and 1 mM EDTA (Sigma Aldrich, cat. no. E5134) for 1 h at RT.

On day 12, for quantification of HPAH phenotypic intracellular or transmembrane markers, cells were fixed with 4% paraformaldehyde (Sigma-Aldrich, cat. no.158127) for 10 min, ice-cold 90% methanol (JT Baker, cat. no. 8045) for 15 min, permeabilized with 1% tritonX-100 (Sigma-Aldrich, cat. no. 93443) PBS pH7.4 (1X) (Gibco, cat. no. 70011-036) supplemented with 1 % BSA (Sigma-Aldrich, cat. no. A9418) for 20 min and stained with the primary antibody CNN1 (Santa Cruz Biotechnology, cat. no. sc-53136, RRID:AB_793529, mouse, 1:50) or ITGA2 (Abcam, cat. no. ab181548, RRID:AB_2847852, rabbit, 1:100) in PBS pH7.4 (1X) (Gibco, cat. no. 70011-036) supplemented with 1 % BSA (Sigma-Aldrich, cat. no. A9418) and 1% tritonX-100 (Sigma-Aldrich, cat. no. 93443) over night at 4 °C. Cells were stained with a secondary antibody anti-rabbit (Cy5, Jackson ImmunoResearch Labs, cat. no. 711-175-152, RRID:AB_2340607, donkey, 1:300) or anti-mouse (AF488, Jackson ImmunoResearch Labs, cat. no. 715-545-151, RRID:AB_2341099, donkey, 1:300) in PBS pH7.4 (1X) (Gibco, cat. no. 70011-036) supplemented with 1 % BSA (Sigma-Aldrich, cat. no. A9418) and 1 % tritonX-100 (Sigma-Aldrich, cat. no. 93443) for 1 h at RT. Flow analysis was performed with the MACSQuant Analyzer 10 and data processing occurred with FlowJo_v10.8.1.

Immunofluorescence staining

Immunofluorescence (IF) staining was performed to visualize characteristic markers of SMCs and HPAH phenotypic markers. For the quantification of HPAH phenotypic markers, freshly differentiated iSMCs were seeded as passage 1 at 7.000 cells/cm^2 on vitronectin-coated (Gibco, cat. no. A31804) chamber slides in 350 µL/cm^2 Essential 6 (DMEM/F12 (ThermoFisher, cat. no. 11330-057), 64 mg/L ascorbic acid 2-phosphate (Sigma-Aldrich, cat. no. A92902), 14 µg/L sodium selenite (Sigma-Aldrich, cat. no. 214485), 543 mg/L sodium bicarbonate (Sigma Aldrich, cat. No. 55761), 20 µg/L Insulin (Sigma-Aldrich, cat. no. I9278), 10.7 µg/mL human recombinant transferrin (Sigma-Aldrich, cat. no. T3705)) with 10 µM Y-27632 (Tocris, cat. no. 1254) and cultivated at 37°C and 5% CO_2 for 24 h. Between day 1-12, every 48 h media was changed to 200 µL/cm^2 E6 with additives of Activin A (Peprotech, cat. no. GMP120-14E, 0.25 ng/ml), sotatercept (MedChemExpress, HY-P99590, 10 µg/ml) or Activin A with sotatercept.

On day 12, for the stainings of actin, CNN1 and TGFβR1 cells were fixed with 4% paraformaldehyde Sigma-Aldrich, cat. no.158127) for 10 min at RT, blocked with 10 % donkey serum (PAN Biotech, cat. no P30-0102) 10 min at RT and stained for actin (Santa Cruz Biotechnology, cat. no. sc-130616, RRID:AB_1561784, mouse, 1:50), CNN1 (Santa Cruz Biotechnology, cat. no. sc-53136, RRID:AB_793529, mouse, 1:50) or TGFβR1 (Thermo Fisher Scientific, cat. no. PA5-142789, RRID:AB_2933432, rabbit, 1:50) ON at 4°C. Cells were stained with a secondary antibody anti-rabbit (Cy5, Jackson ImmunoResearch Labs, cat. no. 711-175-152, RRID:AB_2340607, donkey, 1:300) or anti-mouse (AF488, Jackson

ImmunoResearch Labs, cat. no. 715-545-151, RRID:AB_2341099, donkey, 1:300) for 1 h at RT. Stainings for MYH11, COL1: Cells were fixed with 4% paraformaldehyde (Sigma-Aldrich, cat. no.158127) for 10 min at RT, treated with citrate buffer for 10 min at 95 °C, blocked with 10 % donkey serum (PAN Biotech, cat. no P30-0102) for 10 min at room temperature and stained with MYH11 (Abcam, cat. no. ab133567, RRID:AB_2890982, rabbit, 1:50) or COL1 (Sigma-Aldrich, cat. no. C2456, RRID:AB_476836, mouse, 1:500) ON at 4°C. Cells were stained with a secondary antibody anti-rabbit (Cy5, Jackson ImmunoResearch Labs, cat. no. 711-175-152, RRID:AB_2340607, donkey, 1:300) or anti-mouse ((AF 488, Jackson ImmunoResearch, cat. no. 715-545-151, RRID:AB_2341099, donkey, 1:300) for 1 h at RT. Stainings for ITGA2: Cells were fixed with 4% paraformaldehyde (Sigma-Aldrich, cat. no.158127) for 10 min, ice-cold 90% methanol (JT Baker, cat. no. 8045) for 15 min and permeabilized with 1% tritonX-100 (Sigma-Aldrich, cat. no. 93443) in PBS pH7.4 (1X) (Gibco, cat. no. 70011-036) supplemented with 1 % BSA (Sigma-Aldrich, cat. no. A9418) for 20 min followed by blocking with 10 % donkey serum (PAN Biotech, cat. no P30-0102) for 10 min at RT and stained for ITGA2 (Abcam, cat. no., ab181548, RRID:AB_2847852, rabbit, 1:100) in TBS (pH 7.6, Tris 1X, in-house made) supplemented with 0.2% tritonX-100 (Sigma-Aldrich, cat. no. 93443) and 1 % BSA (Sigma-Aldrich, cat. no. A9418) ON at 4 °C. Cells were stained with a secondary antibody anti-rabbit (Cy5, Jackson ImmunoResearch Labs, cat. no. 711-175-152, RRID:AB_2340607, donkey, 1:300) in 0.2% tritonX-100 (Sigma-Aldrich, cat. no. 93443) in TBS (pH 7.6, Tris 1X, in-house made) supplemented with 1 % BSA (Sigma-Aldrich, cat. no. A9418) for 1 h at RT. All stainings were co-stained for nuclei detection with 0.167 µg/ml DAPI (Sigma Aldrich, cat. no. D9541) for 10 min at RT. IF images were taken with the Zen 2.6 software at the Axioscope 7 microscope (ZEISS) and equally detected in terms of laser intensity, exposure time and sub-sequential image processing.

Western blots

Quantification of total and phosphorylated myosin light chain was performed by western blot analysis. On day 0, freshly differentiated iSMCs were seeded as passage 1 at 20.000 cells/cm^2 on vitronectin-coated (Gibco, cat. no. A31804) plates (Nunc, cat. no. 140675) in 200 µL/cm^2 Essential 6 (DMEM/F12 (ThermoFisher, cat. no. 11330-057), 64 mg/L ascorbic acid 2-phosphate (Sigma-Aldrich, cat. no. A92902), 14 µg/L sodium selenite (Sigma-Aldrich, cat. no. 214485), 543 mg/L sodium bicarbonate (Sigma Aldrich, cat. No. 55761), 20 µg/L Insulin (Sigma-Aldrich, cat. no. I9278), 10.7 µg/mL human recombinant transferrin (Sigma-Aldrich, cat. no. T3705)) with 10 µM Y-27632 (Tocris, cat. no. 1254) and cultivated at 37°C and 5% CO_2 for 24 h. Between day 1-5, every 48 h media was changed to E6 with 200 µL/cm^2. On day 6, media was changed to 200 µL/cm^2 E6 with additives for 1 h: Activin A (Peprotech, cat. no. GMP120-14E, 0.25 ng/ml), sotatercept (MedChemExpress, HY-P99590, 10 µg/ml). Cells were

lyzed and total protein was extracted with (Sigma Aldrich, cat. no. R0278) and protease-phosphatase-inhibitor (Thermo Fisher, cat. no. 78440). After centrifugation at 14.000 g for 20 min at 4°C supernatant was collected and stored at -80°C. The following primary antibodies were used: Vinculin ((Sigma-Aldrich,cat. no. V9131, RRID:AB_477629, mouse, 1:125.000), total myosin light chain (Cell Signaling Technology, cat. no. 8505, RRID:AB_2728760, rabbit, 1:20), phosphorylated myosin light chain (Cell Signaling Technology, cat. no. 3671, RRID:AB_330248, rabbit, 1:50). Western blots were conducted with an automated western blot instrument, Jess ProteinSimple™. The Jess Simple Western system (ProteinSimple, San Jose CA, USA) is an automated, capillary-based immunoassay enabling size-based separation and detection of proteins of interest in low µg quantities. According to the manufacturer's instructions, 2.3 µL of protein lysate was mixed with 0.6 µL of 5x fluorescence master mix and 1 µL 0,1x sample buffer supplied in the standard reagent pack. After denaturation at 95°C for 5 minutes, samples were kept on ice and loaded onto the assay plate together with all required reagents (i.e., antibodies, wash and stripping/replex buffer, luminol/peroxide), followed by centrifugation for 5 minutes at 1,000 *g*. The assay plate and a 12–230 kDa capillary cartridge were loaded into the Jess instrument, where automated separation followed by a chemiluminescence-based immunodetection was completed within 5 hours. Chemiluminescent signals were detected using a CCD camera, and protein expression levels reflected by band intensities were visualized as electropherograms. Densitometric quantification was performed by calculating the area under the curve for each protein of interest using the Compass software (version 7.0.0, ProteinSimple). Normalized expression ratios were calculated as specified in the figure legends.

Collagen assay

Quantification of collagen production was performed by a SiriusRed-based assay. On day 0, freshly differentiated iSMCs were seeded as passage 1 at 15.625 cells/cm^2 on vitronectin-coated (Gibco, cat. no. A31804) plates (Nunc, cat. no. 140675) in 390 µL/cm^2 Essential 6 Essential 6 (DMEM/F12 (ThermoFisher, cat. no. 11330-057), 64 mg/L ascorbic acid 2-phosphate (Sigma-Aldrich, cat. no. A92902), 14 µg/L sodium selenite (Sigma-Aldrich, cat. no. 214485), 543 mg/L sodium bicarbonate (Sigma Aldrich, cat. No. 55761), 20 µg/L Insulin (Sigma-Aldrich, cat. no. I9278), 10.7 µg/mL human recombinant transferrin (Sigma-Aldrich, cat. no. T3705)) with 10 µM Y-27632 (Tocris, cat. no. 1254) and cultivated at 37°C and 5% CO_2 for 24 h. Between day 1 to 5, every 48 h media was changed to 390 µL/cm^2 E6 with additives: Activin A (Peprotech, cat. no. GMP120-14E, 0.25 ng/ml), sotatercept (MedChemExpress, HY-P99590, 10 µg/ml). On day 6, collagen assay was performed as follows: Cells were incubated with 1 µg/ml Hoechst33342 (Thermo Fisher, cat. no. H3570) at 37°C and 5% CO_2 for 1 h and emission was read at 465 nm (9x9 area scan, bottom) with a

plate reader for nuclei counterstain. Cells were fixed with 4% paraformaldehyde (Sigma-Aldrich, cat. no.158127) for 10 min at RT and washed with DPBS (Gibco, cat. no. 14040-091). Cells were stained with SiriusRed (0.1% DirectRed 80 (Sigma Aldrich, cat. no. 365548) in 1% picric acid (Sigma Aldrich, cat. no. P6744)) for 30 min at RT. After three washing steps with HCL (0.01 M), bound SiriusRed was eluated with NaOH (0.1 M). Absorbance was measured at 570 nm with the multimode plate reader (Paradigm, Molecular devices), which is proportional to the amount of fibril collagen.

Proliferation assay

To assess the proliferative capacities a MTT assay was conducted. On day 0, freshly differentiated iSMCs were seeded as passage 1 at 31.250 cells/cm^2 on vitronectin-coated (Gibco, cat. no. A31804) plates (Nunc, cat. no. 140675) in 390 µL/cm^2 Essential 6 (DMEM/F12 (ThermoFisher, cat. no. 11330-057), 64 mg/L ascorbic acid 2-phosphate (Sigma-Aldrich, cat. no. A92902), 14 µg/L sodium selenite (Sigma-Aldrich, cat. no. 214485), 543 mg/L sodium bicarbonate (Sigma Aldrich, cat. No. 55761), 20 µg/L Insulin (Sigma-Aldrich, cat. no. I9278), 10.7 µg/mL human recombinant transferrin (Sigma-Aldrich, cat. no. T3705)) with 10 µM Y-27632 (Tocris, cat. no. 1254) and cultivated at 37°C and 5% CO_2 for 24 h. Between day 1 to 7, every 48 h media was changed to 370 µL/cm^2 E6 with additives: Activin A (Peprotech, cat. no. GMP120-14E, 0.25 ng/ml), sotatercept (MedChemExpress, HY-P99590, 10 µg/ml). On day 8, proliferation assay was performed with the MTT cell proliferation kit (Abcam, cat. no. Ab211091). Cells were treated with 100 µL of a 1:1 mix of the MTT reagent in E6 per well and incubated at 37°C and 5% CO_2 for 3 h. Subsequently, 150 µL of the MTT solvent were added to the MTT reagent in E6 per well and incubated on an orbital shaker at 37°C and 5% CO_2 for 15 min. Solution was gently mixed and absorbance was measured at 590 nm. Values of additive treated wells were normalized to only E6 treated cells per cell line and clone.

Apoptosis assay

The apoptotic rate was analyzed by a caspase-3/7 red assay. On day 0, freshly differentiated iSMCs were seeded as passage 1 at 31.250 cells/cm^2 on vitronectin-coated (Gibco, cat. no. A31804) plates (Nunc, cat. no. 140675) in 390 µL/cm^2 Essential 6 (DMEM/F12 (ThermoFisher, cat. no. 11330-057), 64 mg/L ascorbic acid 2-phosphate (Sigma-Aldrich, cat. no. A92902), 14 µg/L sodium selenite (Sigma-Aldrich, cat. no. 214485), 543 mg/L sodium bicarbonate (Sigma Aldrich, cat. No. 55761), 20 µg/L Insulin (Sigma-Aldrich, cat. no. I9278), 10.7 µg/mL human recombinant transferrin (Sigma-Aldrich, cat. no. T3705)) with 10 µM Y-27632 (Tocris, cat. no. 1254) and cultivated at 37°C and 5% CO_2 for 24 h. On day 1 and 3, media was changed to 370 µL/cm^2 E6 with additives: Activin A (Peprotech, cat. no. GMP120-14E, 0.25 ng/ml), sotatercept (MedChemExpress, HY-P99590, 10 µg/ml). On day 5, caspase staining was

performed with the kit CellEvent™ Caspase-3/7 (ThermoFisher, cat. no. C10431). A 10x working caspase reagent mix was freshly prepared by 1:10 dilution of the 100x stock, combined with 1:10 of HOECHST33342 (Thermo Fisher, cat. no. H3570) for nuclear counterstaining in E6. Then, 14 µL of this 10x mix were added to the preexisting medium of 125 µl per well, leading to an end concentration of 1 µg/ml of HOECHSt33342. Staining mix was gently mixed and incubated for 60 min at 37 °C, 5% CO_2. Fluorescence intensity was measured using a multimode plate reader (Paradigm, Molecular devices). Measurements were performed from the bottom of the 96-well plates to ensure optimal detection of cell-associated signals. For the caspase-3/7 red assay, excitation was set at 585 nm, and emission was recorded at 635 nm with an integration time of 140 ms in monochromatic mode. For nuclear counterstaining with HOECHST33342 (Thermo Fisher, cat. no. H3570), excitation was performed at 360 nm and emission was collected at 465 nm using the same integration time (140 ms) and monochromatic mode. To improve measurement accuracy, both caspase and HOECHST33342 signals were acquired using an AreaScan protocol (9 × 9 reads per well), with HOECHST33342 serving as the nuclear counterstain for normalization.

Contraction assay

The contractility was assessed by a functional collagen-contraction assay. On day 0, freshly differentiated iSMCs were seeded as passage 1 at 20.000 cells/cm^2 on vitronectin-coated (Gibco, cat. no. A31804) plates (Nunc, cat. no. 140675) in 200 µL/cm^2 Essential 6 (DMEM/F12 (ThermoFisher, cat. no. 11330-057), 64 mg/L ascorbic acid 2-phosphate (Sigma-Aldrich, cat. no. A92902), 14 µg/L sodium selenite (Sigma-Aldrich, cat. no. 214485), 543 mg/L sodium bicarbonate (Sigma Aldrich, cat. No. 55761), 20 µg/L Insulin (Sigma-Aldrich, cat. no. I9278), 10.7 µg/mL human recombinant transferrin (Sigma-Aldrich, cat. no. T3705)) with 10 µM Y-27632 (Tocris, cat. no. 1254) and cultivated at 37°C and 5% CO_2 for 24 h. Between day 1-15, every 48 h media was changed to E6 with 200 µL/cm^2 for maturation of iSMCs. On day 16, cells were detached with collagenase for 5 min at 37°C and cell-collagenase-mix was transferred into a tube and shaked at 70 rpm at 37°C for 5 min. Cell suspension was filtered with 100 µm pore size filters (Greiner, cat. no. 542100) and centrifuged at 485 g. Gel matrix was prepared on-ice in the following order for one 48-well (Nunc, cat. no. 150687): 110 µL collagen 13.75 µL PBS pH7.4 (10X) (Gibco, cat. no. 70011-036) incl. phenol red,16.25 µL 0.4 M NaOH, 137.5 µL cell suspension including 450.000 cells. A volume of 250 µL from the gel-cell-mix was added to one 48-well and solidified for 30 min at 37°C and 5% CO_2. After solidification, gel-cell-disc was covered with 0.5 ml of warm E6 and cultivated at 37°C and 5% CO_2 for 24 h. On day 17, media was changed to 0.5 ml E6 with additives: Activin A (Peprotech, cat. no. GMP120-14E, 0.25 ng/ml), sotatercept (MedChemExpress, HY-P99590, 10 µg/ml). The gel disc was released from the edges of the well with a 10 µl pipet tip. Cultivation

was prolonged for another 72 h and shrinkage of gel disc was imaged via brightfield of the Axioscope 7 microscope (ZEISS).

Bulk RNA-sequencing

Transcriptomics was performed by bulk RNA-sequencing. On day 0, fresh differentiated iSMCs were seeded as passage 1 at 15.000 cells/cm^2 on vitronectin-coated (Gibco, cat. no. A31804) plates (Nunc, cat. no. 140675) in 200 µL/cm^2 Essential 6 (DMEM/F12 (ThermoFisher, cat. no. 11330-057), 64 mg/L ascorbic acid 2-phosphate (Sigma-Aldrich, cat. no. A92902), 14 µg/L sodium selenite (Sigma-Aldrich, cat. no. 214485), 543 mg/L sodium bicarbonate (Sigma Aldrich, cat. No. 55761), 20 µg/L Insulin (Sigma-Aldrich, cat. no. I9278), 10.7 µg/mL human recombinant transferrin (Sigma-Aldrich, cat. no. T3705)) with 10 µM Y-27632 (Tocris, cat. no. 1254) and cultivated at 37°C and 5% CO_2 for 24 h. On day 1 and 3, media was changed to E6 with 200 µL/cm^2. On day 5, media was changed to 200 µL/cm^2 E6 with additives: Activin A (Peprotech, cat. no. GMP120-14E, 0.25 ng/ml), sotatercept (MedChemExpress, HY-P99590, 10 µg/ml). On day 7, after 48 h, cells were detached with Accutase™ (Gibco, cat. no. A1110501), lyzed with TRIzol Reagent (Invitrogen, cat. no. 15596018) and isolated with the Nucleospin RNA II Kit (Macherey-Nagel, cat. no. 740955) and stored at -80°C. Bulk RNA-sequencing was performed by Novogene, Germany.

Principle component analysis

Principle component analysis (PCA) analysis for untreated samples was performed based on the Log2(TPM+1)-transformed expression counts using the PCA tools R package. The 2000 most variable genes were identified based on variance across samples and used for dimensionality reduction. Gene expression values were subsequently scaled per gene (row-wise z-score normalization) before PCA.

SMC score analysis

To compare smooth muscle cell (SMC) marker expression scores in Vehicle-treated iSMCs with primary smooth muscle cells and undifferentiated hiPSCs, publicly available RNAseq data from human pulmonary artery smooth muscle cells (PASMCs; GSE144274) and human iPSC lines from the HipSci resource (HPSI0114, https://www.hipsci.org) were used, respectively. Lung vascular SMC marker genes were defined based on the gene set reported by Travaglini et al. (Table 1). For each sample, an SMC score was calculated as the mean expression of Travaglini SMC genes. For primary PASMC and hiPSC derived SMC samples, variance-stabilized expression values obtained using DESeq2 were used, and SMC scores were computed as the mean VST expression across SMC genes per sample. For external hiPSC samples, transcript-level abundance estimates in TPM were aggregated to gene-level expression based on HGNC gene symbols, and SMC scores were calculated as the mean

log2(TPM + 1) expression across SMC genes per sample. SMC scores were compared across sample groups using violin and box plots to visualize the distribution of SMC gene-set expression.

Hallmark/marker gene set scoring

For hallmark gene set scoring, bulk RNAseq expression values were analyzed in R (v4.5.0) using a gene-by-sample FPKM matrix. Gene symbols were used as identifiers; when multiple rows mapped to the same gene symbol, values were merged by taking the mean FPKM per sample. Sample names were parsed into genotype, replicate, and treatment metadata to generate a sample annotation table. To visualize gene set-associated expression changes across conditions, samples were grouped by genotype and treatment, and gene expression was averaged across biological replicates within each group (row-wise mean across samples). For each genotype, treatment-induced gene expression level changes were quantified relative to the corresponding vehicle control by computing log2 fold-changes with a small pseudo-count (1×10^{-6}) to avoid division by zero. For heatmap gene ordering, genes were classified into two predefined, manually curated subsets representing genes selected to be positively supporting or opposing the corresponding gene set or hallmark signature, where applicable. Within each predefined subset, genes were hierarchically clustered based on the fold-change matrix and the final gene order for heatmap visualization was obtained by concatenating the clustered order of the positively supporting gene subset followed by the opposing gene subset. Row-wise z-score normalization was performed across all displayed conditions or across each genotypes before visualization, genes with zero variance were assigned a z-score of 0. Heatmaps were rendered using ggplot2 geom_tile with a diverging colour scale centred at zero, and gene labels were annotated to indicate membership in the predefined gene subsets.

Table 1: All listed gene sets are publicly available from the Molecular Signatures Database (MSigDB).

Name gene set	Data bank	ID	Version	Organism
TRAVAGLINI_LUNG_VASCULAR_SMOOTH_MUSCLE_CELL	Molecular Signatures Database (MSigDB	MSigDB: M41672	MSigDB: 7.3	Homo sapiens
GOBP_SMOOTH_MUSCLE_CONTRACTION	Molecular Signatures Database	MSigDB: M13593 GO: 0006939	MSigDB: 2025.1 (Hs) Go-Release: 2025-03-16	Homo sapiens

	(MSigDB)			
REACTOME_SMOOTH_MUSCLE_CONTRACTION	Molecular Signatures Database (MSigDB)	MSigDB: M1429 REACTOME: R-HSA-445355	MSigDB: 2025.1 (Hs) REACTOME: 92	Homo sapiens
CELL_PROLIFERATION_GO_0008283	Molecular Signatures Database (MSigDB)	MSigDB: M16210 GO:0008283	MSigDB: 5.2	Homo sapiens
GOBP_EXTRACELLULAR_MATRIX_ASSEMBLY	Molecular Signatures Database (MSigDB)	MSigDB: M11366 GO:0085029	MSigDB: 2025.1 (Hs) GO Release 2025-03-16.	Homo sapiens
HALLMARK_APOPTOSIS	Molecular Signatures Database (MSigDB)	MSigDB: M5902	MSigDB: 5.0	Homo sapiens

Functional enrichment analysis

Functional enrichment analysis of the gene sets was performed using Enrichr. Cell type enrichment was evaluated using the CellMarker 2024. Enrichment results were visualized using bar plots generated by Enrichr [82].

Myofibroblast signature scoring and expression comparison

A myofibroblast signature score “Myoscore” was calculated from the bulk RNA-seq FPKM expression matrix using a predefined, manually curated set of myofibroblast-associated marker genes with R (v4.5.0). Gene symbols were used as identifiers; if multiple rows mapped to the same gene symbol, values were merged by taking the mean FPKM per sample. After removing duplicated gene symbols from the marker list, only genes present in the expression matrix were retained. Myoscore distributions across groups were visualized using boxplots containing median, the interquartile range (IQR), and whiskers = 1.5 × IQR with overlaid jittered

points representing individual biological replicates. For heatmap visualization, gene expression was averaged across biological replicates within each genotype–treatment group, and treatment-associated changes were quantified as log2 fold-changes relative to the corresponding vehicle control within each genotype, using a small pseudo-count (1×10^{-6}) to avoid division by zero. Genes were hierarchically clustered based on the fold-change matrix to define the heatmap row order. Row-wise z-score normalization ($z = (x - \text{mean})/\text{sd}$) was performed across all displayed conditions prior to visualization, genes with zero variance were assigned z = 0, and heatmaps were rendered using ggplot2 geom_tile with a diverging color scale centered at zero.

To validate Myoscore result, we generated a myofibroblast gene set that is less dependent on subjective manual selection. We leveraged three independently annotated human lung single-cell RNA-seq datasets: GSE135893, GSE136831 and the Munich cohort dataset from Mayr et al, 2021. In each dataset, author-provided cell type annotations were used to define cell identities. Within each dataset, differential expression analysis was performed comparing myofibroblasts against all other cell types using Seurat's FindMarkers function. To ensure robustness to feature selection, marker detection was conducted both across all genes and restricted to highly variable genes, and the resulting myofibroblast-enriched genes (padj < 0.05 and avg_log2FC > 0) were merged and de-duplicated. Candidate genes were further filtered for expression prevalence, retaining only those detected in at least 30% of myofibroblast cells.

To quantify cell-type specificity, a specificity score was calculated for each candidate gene as the difference between its mean expression in myofibroblasts and the maximum mean expression observed across all non-myofibroblast cell types. This specificity metric was combined with the differential expression effect size to derive a composite ranking score (0.7 × specificity score + 0.3 × avg_log2FC), and the top 100 genes per dataset were selected as data-driven myofibroblast marker sets. Marker gene lists derived independently from the three datasets were then compared, and the final myofibroblast gene set was defined as genes identified in at least two of the three datasets, representing the most consistent cross-dataset signature. The myofibroblast gene set was subsequently used for module score-based validation in all three single-cell datasets to confirm its robust and selective enrichment in myofibroblast populations across datasets and analytical frameworks, after which this gene set was used for myofibroblast signature scoring as validation to the results previously generated.

Data availability

All data will be made publicly available upon publication.

Author contributions

A.S. performed and analyzed experiments and wrote the manuscript, L.C., L M., G.B., C.P., T.K., J.B. performed experiments, Y. W., C. V., A.K. performed data analysis, A. W. performed data analysis and provided scientific input, R.S., A.R. provided scientific input, J. C. K., M. M. H. provided patient samples and scientific input, RO, and UM conceptualized and supervised the study, provided scientific input and wrote the manuscript. All authors reviewed and approved the final version of the manuscript.

Conflict of interest

MMH has received fees for consultations or lectures from 35Pharma, Acceleron, Actelion, Aerovate, AOP Health, Bayer, Ferrer, Gossamer, Inhibikase, Janssen, Keros, MSD and Novartis.

Acknowledgments

The authors would like to thank G. Hansmann for his help with sample collection.

Funding

This work was supported by the German Center for Lung Research (DZL; 82DZL002C1) and the German Research Foundation OL 653/2-1 (RO). Lower Saxony (Nachhaltigkeitsfinanzierung Exzellenzcluster REBIRTH, ZN3440),German Research Foundation (DFG KFO311, MA 2331/18-1, MA 2331/18-2) (UM)

References

1. Preston, I.R.*, et al.* A long-term follow-up study of sotatercept for treatment of pulmonary arterial hypertension: interim results of SOTERIA. *Eur Respir J* **66**(2025).
2. Zolty, R. Antiproliferative therapies in pulmonary arterial hypertension. *Expert Opin Pharmacother* **26**, 1895-1911 (2025).
3. Yun, X.*, et al.* Aquaporin 1 confers apoptosis resistance in pulmonary arterial smooth muscle cells from the SU5416 hypoxia rat model. *Physiol Rep* **12**, e16156 (2024).
4. Wilson, J.L.*, et al.* Unraveling endothelin-1 induced hypercontractility of human pulmonary artery smooth muscle cells from patients with pulmonary arterial hypertension. *PLOS ONE* **13**, e0195780 (2018).
5. Thenappan, T., Chan, S.Y. & Weir, E.K. Role of extracellular matrix in the pathogenesis of pulmonary arterial hypertension. *Am J Physiol Heart Circ Physiol* **315**, H1322-h1331 (2018).

6. Mutgan, A.C*., et al.* A comprehensive map of proteoglycan expression and deposition in the pulmonary arterial wall in health and pulmonary hypertension. *American Journal of Physiology-Lung Cellular and Molecular Physiology* **327**, L173-L188 (2024).
7. Eichstaedt, C.A*., et al.* Gene panel diagnostics reveals new pathogenic variants in pulmonary arterial hypertension. *Respir Res* **23**, 74 (2022).
8. Evans, J.D*., et al.* BMPR2 mutations and survival in pulmonary arterial hypertension: an individual participant data meta-analysis. *Lancet Respir Med* **4**, 129-137 (2016).
9. Yung, L.M*., et al.* ACTRIIA-Fc rebalances activin/GDF versus BMP signaling in pulmonary hypertension. *Sci Transl Med* **12**(2020).
10. Ryanto, G.R.T., Musthafa, A., Hara, T. & Emoto, N. Inactivating the Uninhibited: The Tale of Activins and Inhibins in Pulmonary Arterial Hypertension. *Int J Mol Sci* **24**(2023).
11. Soon, E*., et al.* Bone morphogenetic protein receptor type II deficiency and increased inflammatory cytokine production. A gateway to pulmonary arterial hypertension. *Am J Respir Crit Care Med* **192**, 859-872 (2015).
12. Guignabert, C*., et al.* Serum and Pulmonary Expression Profiles of the Activin Signaling System in Pulmonary Arterial Hypertension. *Circulation* **147**, 1809-1822 (2023).
13. Manzi, G*., et al.* The pleiotropic effects of sotatercept. *Vascul Pharmacol*, 107577 (2025).
14. Humbert, M*., et al.* Sotatercept for the treatment of pulmonary arterial hypertension: PULSAR open-label extension. *Eur Respir J* **61**(2023).
15. Andre, P*., et al.* Therapeutic Approaches for Treating Pulmonary Arterial Hypertension by Correcting Imbalanced TGF-beta Superfamily Signaling. *Front Med (Lausanne)* **8**, 814222 (2021).
16. Hoeper, M.M*., et al.* Phase 3 Trial of Sotatercept for Treatment of Pulmonary Arterial Hypertension. *N Engl J Med* **388**, 1478-1490 (2023).
17. Guignabert, C*., et al.* Pathology and pathobiology of pulmonary hypertension: current insights and future directions. *European Respiratory Journal* **64**, 2401095 (2024).
18. Boucherat, O., Agrawal, V., Lawrie, A. & Bonnet, S. The Latest in Animal Models of Pulmonary Hypertension and Right Ventricular Failure. *Circ Res* **130**, 1466-1486 (2022).
19. Gu, M*., et al.* Patient-Specific iPSC-Derived Endothelial Cells Uncover Pathways that Protect against Pulmonary Hypertension in BMPR2 Mutation Carriers. *Cell Stem Cell* **20**, 490-504 e495 (2017).
20. Sa, S*., et al.* Induced Pluripotent Stem Cell Model of Pulmonary Arterial Hypertension Reveals Novel Gene Expression and Patient Specificity. *Am J Respir Crit Care Med* **195**, 930-941 (2017).
21. Stenmark, K.R., Frid, M.G., Graham, B.B. & Tuder, R.M. Dynamic and diverse changes in the functional properties of vascular smooth muscle cells in pulmonary hypertension. *Cardiovasc Res* **114**, 551-564 (2018).
22. McLaughlin, V.V*., et al.* ACCF/AHA 2009 expert consensus document on pulmonary hypertension a report of the American College of Cardiology Foundation Task Force on Expert Consensus Documents and the American Heart Association developed in collaboration with the American College of Chest Physicians; American Thoracic Society, Inc.; and the Pulmonary Hypertension Association. *J Am Coll Cardiol* **53**, 1573-1619 (2009).
23. Dai, J., Chen, H., Fang, J., Wu, S. & Jia, Z. Vascular Remodeling: The Multicellular Mechanisms of Pulmonary Hypertension. *Int J Mol Sci* **26**(2025).
24. Humbert, M*., et al.* Sotatercept for the Treatment of Pulmonary Arterial Hypertension. *N Engl J Med* **384**, 1204-1215 (2021).
25. Yu, J., Wilson, J., Taylor, L. & Polgar, P. DNA microarray and signal transduction analysis in pulmonary artery smooth muscle cells from heritable and idiopathic pulmonary arterial hypertension subjects. *J Cell Biochem* **116**, 386-397 (2015).
26. Zhou, H*., et al.* MKI67 as a potential diagnostic biomarker in pulmonary hypertension. *Front Pediatr* **10**, 1016889 (2022).
27. Crnkovic, S*., et al.* Single-cell transcriptomics reveals skewed cellular communication and phenotypic shift in pulmonary artery remodeling. *JCI Insight* **7**(2022).

28. Wang, W.*, et al.* Comparative Transcriptional Analysis of Pulmonary Arterial Hypertension Associated With Three Different Diseases. *Front Cell Dev Biol* **9**, 672159 (2021).
29. Ma, L. & Chung, W.K. The role of genetics in pulmonary arterial hypertension. *J Pathol* **241**, 273-280 (2017).
30. Lagna, G., Nguyen, P.H., Ni, W. & Hata, A. BMP-dependent activation of caspase-9 and caspase-8 mediates apoptosis in pulmonary artery smooth muscle cells. *American Journal of Physiology-Lung Cellular and Molecular Physiology* **291**, L1059-L1067 (2006).
31. Christou, H. & Khalil, R.A. Mechanisms of pulmonary vascular dysfunction in pulmonary hypertension and implications for novel therapies. *Am J Physiol Heart Circ Physiol* **322**, H702-h724 (2022).
32. Barnes, E.A., Chen, C.H., Sedan, O. & Cornfield, D.N. Loss of smooth muscle cell hypoxia inducible factor-1α underlies increased vascular contractility in pulmonary hypertension. *Faseb j* **31**, 650-662 (2017).
33. Lyle, M.A., Davis, J.P. & Brozovich, F.V. Regulation of Pulmonary Vascular Smooth Muscle Contractility in Pulmonary Arterial Hypertension: Implications for Therapy. *Front Physiol* **8**, 614 (2017).
34. Winder, S.J., Allen, B.G., Clement-Chomienne, O. & Walsh, M.P. Regulation of smooth muscle actin-myosin interaction and force by calponin. *Acta Physiol Scand* **164**, 415-426 (1998).
35. Konik, E.A., Han, Y.S. & Brozovich, F.V. The role of pulmonary vascular contractile protein expression in pulmonary arterial hypertension. *J Mol Cell Cardiol* **65**, 147-155 (2013).
36. Huang, L.*, et al.* Transgelin as a potential target in the reversibility of pulmonary arterial hypertension secondary to congenital heart disease. *J Cell Mol Med* **22**, 6249-6261 (2018).
37. Huang, C.H., Schuring, J., Skinner, J.P., Mok, L. & Chong, M.M.W. MYL9 deficiency is neonatal lethal in mice due to abnormalities in the lung and the muscularis propria of the bladder and intestine. *PLoS One* **17**, e0270820 (2022).
38. Rensen, S.S.*, et al.* Smoothelin-B deficiency results in reduced arterial contractility, hypertension, and cardiac hypertrophy in mice. *Circulation* **118**, 828-836 (2008).
39. Jimenez, S.A. & Piera-Velazquez, S. Endothelial to mesenchymal transition (EndoMT) in the pathogenesis of Systemic Sclerosis-associated pulmonary fibrosis and pulmonary arterial hypertension. Myth or reality? *Matrix Biology* **51**, 26-36 (2016).
40. Morrell, N.W.*, et al.* Cellular and molecular basis of pulmonary arterial hypertension. *J Am Coll Cardiol* **54**, S20-S31 (2009).
41. Ranchoux, B.*, et al.* Endothelial-to-mesenchymal transition in pulmonary hypertension. *Circulation* **131**, 1006-1018 (2015).
42. Darby, I.A., Zakuan, N., Billet, F. & Desmouliere, A. The myofibroblast, a key cell in normal and pathological tissue repair. *Cell Mol Life Sci* **73**, 1145-1157 (2016).
43. Padrez, Y.*, et al.* Quantitative and qualitative analysis of pulmonary arterial hypertension fibrosis using wide-field second harmonic generation microscopy. *Scientific Reports* **12**, 7330 (2022).
44. Wei, L.*, et al.* Serotonylated fibronectin is elevated in pulmonary hypertension. *Am J Physiol Lung Cell Mol Physiol* **302**, L1273-1279 (2012).
45. Ihida-Stansbury, K.*, et al.* Tenascin-C is induced by mutated BMP type II receptors in familial forms of pulmonary arterial hypertension. *Am J Physiol Lung Cell Mol Physiol* **291**, L694-702 (2006).
46. Biasin, V.*, et al.* PDGFRalpha and alphaSMA mark two distinct mesenchymal cell populations involved in parenchymal and vascular remodeling in pulmonary fibrosis. *Am J Physiol Lung Cell Mol Physiol* **318**, L684-L697 (2020).
47. Walsh, S.M.*, et al.* Novel differences in gene expression and functional capabilities of myofibroblast populations in idiopathic pulmonary fibrosis. *Am J Physiol Lung Cell Mol Physiol* **315**, L697-L710 (2018).
48. Wu, S.*, et al.* The gene expression of CALD1, CDH2, and POSTN in fibroblast are related to idiopathic pulmonary fibrosis. *Front Immunol* **15**, 1275064 (2024).

49. Choo, Y.Y.*, et al.* Calponin 1 contributes to myofibroblast differentiation of human pleural mesothelial cells. *Am J Physiol Lung Cell Mol Physiol* **322**, L348-L364 (2022).
50. Katoh, D.*, et al.* Tenascin-C Induces Phenotypic Changes in Fibroblasts to Myofibroblasts with High Contractility through the Integrin alphavbeta1/Transforming Growth Factor beta/SMAD Signaling Axis in Human Breast Cancer. *Am J Pathol* **190**, 2123-2135 (2020).
51. Dai, Y.*, et al.* MFAP5 as a promising biomarker for connective tissue disease-associated interstitial lung disease. *Front Immunol* **16**, 1642408 (2025).
52. Zhao, Q.*, et al.* The insulin-like growth factor binding protein-microfibrillar associated protein-sterol regulatory element binding protein axis regulates fibroblast-myofibroblast transition and cardiac fibrosis. *Br J Pharmacol* **181**, 2492-2508 (2024).
53. Pan, Y.S.*, et al.* Exploration of upstream and downstream mechanisms of the TAGLN2 gene in pulmonary arterial hypertension. *Medicine (Baltimore)* **104**, e45295 (2025).
54. Jia, M.*, et al.* Early events marking lung fibroblast transition to profibrotic state in idiopathic pulmonary fibrosis. *Respir Res* **24**, 116 (2023).
55. Bertero, T., Handen, A.L. & Chan, S.Y. Factors Associated with Heritable Pulmonary Arterial Hypertension Exert Convergent Actions on the miR-130/301-Vascular Matrix Feedback Loop. *Int J Mol Sci* **19**(2018).
56. Umesh, A., Paudel, O., Cao, Y.N., Myers, A.C. & Sham, J.S. Alteration of pulmonary artery integrin levels in chronic hypoxia and monocrotaline-induced pulmonary hypertension. *J Vasc Res* **48**, 525-537 (2011).
57. Hiepen, C., Mendez, P.L. & Knaus, P. It Takes Two to Tango: Endothelial TGFbeta/BMP Signaling Crosstalk with Mechanobiology. *Cells* **9**(2020).
58. Morgan Huse, T.W.M., 2 Ye-Guang Chen,3,6 & Massague´, a.J. The TGF℔ Receptor Activation Process: An Inhibitor- to Substrate-Binding Switch. *Molecular Cell* **Vol. 8**, 671–682 (2001).
59. Jumaar, C.*, et al.* In vitro models and approaches to study underlying pathways of pulmonary arterial hypertension: a review. *Biochem Biophys Res Commun* **781**, 152503 (2025).
60. Ma, B.*, et al.* Pulmonary artery smooth muscle cell phenotypic switching: A key event in the early stage of pulmonary artery hypertension. *Drug Discovery Today* **28**, 103559 (2023).
61. Yuan, J.X.J. & Rubin, L.J. Pathogenesis of Pulmonary Arterial Hypertension. *Circulation* **111**, 534-538 (2005).
62. Phan, S.H. The Myofibroblast in Pulmonary Fibrosis. *J Am Heart Assoc* (2023).
63. Chen, R., McVey, D.G., Shen, D., Huang, X. & Ye, S. Phenotypic Switching of Vascular Smooth Muscle Cells in Atherosclerosis. *J Am Heart Assoc* **12**, e031121 (2023).
64. Merfeld-Clauss, S., Lu, H., Wu, X., March, K.L. & Traktuev, D.O. Hypoxia-induced activin A diminishes endothelial cell vasculogenic activity. *J Cell Mol Med* **22**, 173-184 (2018).
65. Upton, P.D., Davies, R.J., Trembath, R.C. & Morrell, N.W. Bone morphogenetic protein (BMP) and activin type II receptors balance BMP9 signals mediated by activin receptor-like kinase-1 in human pulmonary artery endothelial cells. *J Biol Chem* **284**, 15794-15804 (2009).
66. Chu, K.Y., Malik, A., Thamilselvan, V. & Martinez-Hackert, E. Type II BMP and activin receptors BMPR2 and ACVR2A share a conserved mode of growth factor recognition. *J Biol Chem* **298**, 102076 (2022).
67. Goto, K., Kamiya, Y., Imamura, T., Miyazono, K. & Miyazawa, K. Selective inhibitory effects of Smad6 on bone morphogenetic protein type I receptors. *J Biol Chem* **282**, 20603-20611 (2007).
68. Masao Takase, T.I., * T. Kuber Sampath,† Kohsuke Takeda,* Hidenori Ichijo,* Kohei Miyazono,* and Masahiro Kawabat. nduction of Smad6 mRNA by Bone Morphogenetic Proteins. *BIOCHEMICAL AND BIOPHYSICAL RESEARCH COMMUNICATIONS* **244, 26–29** ((1998)).
69. Hiepen, C.*, et al.* BMPR2 acts as a gatekeeper to protect endothelial cells from increased TGFbeta responses and altered cell mechanics. *PLoS Biol* **17**, e3000557 (2019).
70. Chaikuad, A., Thangaratnarajah, C., von Delft, F. & Bullock, A.N. Structural consequences of BMPR2 kinase domain mutations causing pulmonary arterial hypertension. *Scientific Reports* **9**, 18351 (2019).

71. John, A., Kizhakkedath, P., Al-Gazali, L. & Ali, B.R. Defective cellular trafficking of the bone morphogenetic protein receptor type II by mutations underlying familial pulmonary arterial hypertension. *Gene* **561**, 148-156 (2015).
72. Sobolewski, A.*, et al.* Failure of bone morphogenetic protein receptor trafficking in pulmonary arterial hypertension: potential for rescue. *Hum Mol Genet* **17**, 3180-3190 (2008).
73. Hirata, H.*, et al.* Actomyosin bundles serve as a tension sensor and a platform for ERK activation. *EMBO Rep* **16**, 250-257 (2015).
74. Garamszegi, N.*, et al.* Extracellular matrix-induced transforming growth factor-beta receptor signaling dynamics. *Oncogene* **29**, 2368-2380 (2010).
75. Wada, W., Kuwano, H., Hasegawa, Y. & Kojima, I. The dependence of transforming growth factor-beta-induced collagen production on autocrine factor activin A in hepatic stellate cells. *Endocrinology* **145**, 2753-2759 (2004).
76. Yuan, C., Ni, L. & Wu, X. Activin A activation drives renal fibrosis through the STAT3 signaling pathway. *Int J Biochem Cell Biol* **134**, 105950 (2021).
77. Staudacher, J.J.*, et al.* Activin signaling is an essential component of the TGF-beta induced pro-metastatic phenotype in colorectal cancer. *Sci Rep* **7**, 5569 (2017).
78. Vaughan, M.B., Howard, E.W. & Tomasek, J.J. Transforming growth factor-beta1 promotes the morphological and functional differentiation of the myofibroblast. *Exp Cell Res* **257**, 180-189 (2000).
79. Wipff, P.J., Rifkin, D.B., Meister, J.J. & Hinz, B. Myofibroblast contraction activates latent TGF-beta1 from the extracellular matrix. *J Cell Biol* **179**, 1311-1323 (2007).
80. Yan, Y.*, et al.* Elevated levels of plasma transforming growth factor-β1 in idiopathic and heritable pulmonary arterial hypertension. *Int J Cardiol* **222**, 368-374 (2016).
81. Savale, L.*, et al.* Effect of sotatercept on circulating proteomics in pulmonary arterial hypertension. *Eur Respir J* **64**(2024).
82. Kuleshov, M.V.*, et al.* Enrichr: a comprehensive gene set enrichment analysis web server 2016 update. *Nucleic Acids Res* **44**, W90-97 (2016).